Cellular/Molecular

Deletion of CPEB3 Enhances Hippocampus-Dependent Memory via Increasing Expressions of PSD95 and NMDA Receptors

Hsu-Wen Chao,[1]* Li-Yun Tsai,[1]* Yi-Ling Lu,[1] Pei-Yi Lin,[1] Wen-Hsuan Huang,[1] Hsin-Jung Chou,[1] Wen-Hsin Lu,[1,2] Hsiu-Chen Lin,[1] Ping-Tao Lee,[1] and Yi-Shuian Huang[1,2]

[1]Institute of Biomedical Sciences, Academia Sinica, Taipei 115, Taiwan and [2]Taiwan International Graduate Program, National Yang-Ming University, Taipei 112, Taiwan

Long-term memory requires activity-dependent synthesis of plasticity-related proteins (PRPs) to strengthen synaptic efficacy and consequently consolidate memory. Cytoplasmic polyadenylation element binding protein (CPEB)3 is a sequence-specific RNA-binding protein that regulates translation of several PRP RNAs in neurons. To understand whether CPEB3 plays a part in learning and memory, we generated CPEB3 knock-out (KO) mice and found that the null mice exhibited enhanced hippocampus-dependent, short-term fear memory in the contextual fear conditioning test and long-term spatial memory in the Morris water maze. The basal synaptic transmission of Schaffer collateral-CA1 neurons was normal but long-term depression evoked by paired-pulse low-frequency stimulation was modestly facilitated in the juvenile KO mice. Molecular and cellular characterizations revealed several molecules in regulating plasticity of glutamatergic synapses are translationally elevated in the CPEB3 KO neurons, including the scaffolding protein PSD95 and the NMDA receptors along with the known CPEB3 target, GluA1. Together, CPEB3 functions as a negative regulator to confine the strength of glutamatergic synapses by downregulating the expression of multiple PRPs and plays a role underlying certain forms of hippocampus-dependent memories.

Introduction

Modulation of long-lasting synaptic strength requires activity-induced synthesis of plasticity-related proteins (PRPs) to sustain morphological and functional changes of synapses that are crucial for the establishment and consolidation of long-term memory (LTM). Several RNA-binding proteins control specific PRP syntheses in neurons via regulating RNA transport, translation, and/ or stability; and when genetically mutated or ablated, results in aberrant memory performance in humans and mice (Richter and Klann, 2009; for review, see Costa-Mattioli et al., 2009; Darnell and Richter, 2012; Gal-Ben-Ari et al., 2012). Cytoplasmic polyadenylation element binding protein (CPEB) family of RNA-binding proteins in vertebrates contains four members, CPEBs1–4, all of which are expressed in the brain (Theis et al., 2003) and share structure and sequence identity in the RNA-binding domain (RBD; Huang et al., 2006). Disruption of *cpeb1* gene in mice reduced extinction of hippocampus-dependent LTM (Berger-Sweeney et al., 2006) and altered synaptic electrophysiology in the Schaffer collateral (SC) pathway (Alarcon et al., 2004). In contrast, the contribution of other CPEB members in learning and memory is not clear. Among them, CPEB3 was shown to repress the translation of several PRP RNAs, which encode for epidermal growth factor receptor and the subunits of AMPA receptor (AMPAR), GluA1, and GluA2 (Huang et al., 2006; Peng et al., 2010; Pavlopoulos et al., 2011). NMDA receptor (NMDAR) signaling triggers calpain 2-mediated cleavage of CPEB3 and subsequently results in translation of CPEB3-targeted RNAs (Huang et al., 2006; Chen and Huang, 2012; Wang and Huang, 2012). In this model, CPEB3 is a repressor and ameliorates its repression ability via NMDAR-activated proteolysis. Moreover, monoubiquitination of CPEB3 by neuralized1 (Neurl1) can switch CPEB3 from a repressor to an activator to increase the translation of GluA1 and GluA2 RNAs (Pavlopoulos et al., 2011). Thus, CPEB3 bilaterally regulates translation depending on its ubiquitin-modified state. Although there are a couple of mechanisms identified to modulate CPEB3-repressed translation in neurons, the role of CPEB3 in learning and memory is not clear. Thus, we generated CPEB3 knock-out (KO) mice, which demonstrated normal physical performance and home-cage behaviors, but showed reduced exploratory activity in the

Received July 18, 2013; revised Sept. 1, 2013; accepted Sept. 18, 2013.

Author contributions: H.-W.C., L.-Y.T., and Y.-S.H. designed research; H.-W.C., L.-Y.T., Y.-L.L., P.-Y.L., W.-H.H., H.-J.C., W.-H.L., H.-C.L., P.-T.L., and Y.-S.H. performed research; H.-W.C., L.-Y.T., Y.-L.L., P.-Y.L., W.-H.H., H.-J.C., W.-H.L., and Y.-S.H. analyzed data; Y.-S.H. wrote the paper.

This work was supported by National Science Council [NSC 99-2311-B-001-020-MY3] and Academia Sinica [AS-100-TP-B09] in Taiwan. We thank the Taiwan Mouse Clinic, which is funded by the National Research Program for Biopharmaceuticals from the NSC, for conducting the home-cage experiments and SHIRPA modified assays. We appreciate Ching-Pang Chang for assistance on the behavior study, the transgenic core facility for embryonic stem cell gene targeting, and blastocyst microinjection and Su-Ping Lee and Huei-Fang Wu in the IMB cores for helping confocal and calcium image analyses. We thank Drs. Lih-Chu Chiou, Po-Wu Gean, Kuei-Sen Hsu, and Ming-Yuan Min for their assistance setting up the field recording system.

*H.-W.C. and L.-Y.T. contributed equally to this work.

The authors declare no competing financial interests.

Correspondence should be addressed to Yi-Shuian Huang, Institute of Biomedical Sciences, Academia Sinica, 128 Section 2, Academia Road, Taipei 11529, Taiwan. E-mail: yishuian@ibms.sinica.edu.tw.

DOI:10.1523/JNEUROSCI.3043-13.2013

 0270-6474/13/3317008-15$15.00/0

open field. The learning and memory abilities were assessed using contextual fear conditioning and Morris water maze. In the former assay, the KO animals showed elevated short-term fear responses during acquisition and extinction trainings, but exhibited normal long-term fear memory. In the latter task, the null mice displayed better consolidated spatial memory, which appeared to hinder their ability to locate a new platform position in the reversal probe test. Electro-recordings identified enhanced paired-pulse low-frequency stimulation (PP-LFS)-induced long-term depression (LTD) at the SC-CA1 synapses of KO mice. Molecular and cellular characterizations revealed that the enlargement of dendritic spines and elevated expression of several PRPs, including GluA1, NMDARs, and PSD95, in the KO neurons. The protein, but not the RNA level of these CPEB3 targets, was elevated, which was accompanied by a shift of the RNA distribution toward polysomes in the KO brains. These results revealed the *in vivo* role of CPEB3 as a negative regulator to constrain the translation of multiple PRP RNAs and the strength of consolidated memory.

Materials and Methods

Antibodies and chemicals

Antibodies used in the study were as follows: myc-tag and LRP130 from Santa Cruz Biotechnology; NR1, NR2A, NR2B, GluA1, PSD95, and synaptophysin from Millipore; and GFP, β-actin, and α-tubulin from Sigma-Aldrich. The CPEB3 antibodies have been described previously (Chao et al., 2012; Wang and Huang, 2012). Alexa Fluor-conjugated secondary antibodies were obtained from Invitrogen. With the exception of the Fura-2 AM calcium indicator (Invitrogen), all of the other chemicals were purchased from Sigma-Aldrich.

Animals

All of the experimental protocols were performed in accordance with the guidelines of the Institutional Animal Care and Utilization Committee. C57BL/6J mice were housed under a 12 h light/dark cycle in a climate-controlled room with *ad libitum* access to food and water. All efforts were made to minimize the number of animals used and their suffering. The wild-type (WT) and KO male mice used for behavior, electrophysiology, and biochemical studies were littermates from heterozygous matings.

Construction of the CPEB3 targeting vector and generation of mutant mice

The genomic BAC clone (RP23-56A17) containing the 5′-portion of the C57BL/6J mouse CPEB3 gene was used to construct the targeting vector by the recombineering technique according to the manufacturer's instructions (Gene Bridges). Briefly, a loxP-Neo-loxP cassette was first recombined into the 3′-end of exon 2 and excised with recombinant Cre (New England Biolabs) *in vitro* to result in a single loxP site. The resulting plasmid was recombineered with the Frt-PGK-Neo-Frt-loxP cassette to the 5′-end of exon 2. The plasmid was linearized with NruI and electroporated into C57BL/6J ES cells. Four correct clones of 258 G418-resistant clones were injected into c2J blastocysts. Only one clone derived a germline-transmitted line. The mouse carrying floxed allele was first crossed with Frt recombinase driven by the β-actin promoter to remove the Frt-PGK-Neo-Frt cassette. The resulting line was maintained as fCPEB3 mice and then crossed with the protamine-Cre transgenic mouse to derive KO mice.

Genotyping of CPEB3 embryos and mice

The genotypes were determined by PCR using tail biopsies and the KAPA mouse genotyping kit (KAPA Biosystems). Briefly, tail samples were lysed in 20 μl of KAPA extract buffer for 20 min at 75°C and then 5 min at 95−100°C. The DNA sample was then diluted with 60 μl of H_2O, and 0.5 μl was used for a 10 μl PCR reaction. The sense primer, CP3F1 5′-TTTGATCCTTCTGCCTCTCCCTC-3′ and two antisense primers, CP3R1 5′-TTGGTACACGACCCTCTTTCCCC-3′ and CP3R2 5′-TATGGCTCTGAAGGTCGTGTCCT-3′ at a 2:1:1 ratio were used to amplify the WT and KO alleles, respectively.

Primary neuronal cultures, DNA transfection, and lentivirus infection

To culture WT and KO neurons, the cortices and hippocampi of E18 embryos from heterozygous matings were isolated and maintained individually in HBSS for 2 h on ice. At the same time, the tails were collected for genotyping. Once the genotypes were determined, the WT and KO cerebral cortices regardless of sex were pooled and used for neuronal cultures as previously described (Chao et al., 2012). The cell density was at 3×10^5 cells/ well in a 12-well plate, 2×10^6 cells/60 mm dish, and 5×10^6 cells/100 mm dish. Delivery of DNA into the neurons was performed using calcium phosphate transfection or lentivirus infection as previously reported (Chao et al., 2012).

Immunohistochemistry, immunofluorescence staining, imaging acquisition, and quantification

Coronal sections of WT and KO male brains after 10 min fixation in 4% formaldehyde and 20 min antigen retrieval in 10 mM sodium citrate buffer, pH 6 at 70°C, were washed twice with Tris-buffered saline (TBS) and permeabilized with 0.2% Triton X-100 in TBS. After three washes with TBS and 1 h blocking in 10% horse serum, the slices were incubated with affinity-purified CPEB3 antibody at 4°C overnight. After washes with TBS, the immunobinding signal was developed using the Vectastain Elite ABC kit (Vector Laboratories) following the manufacturer's protocol. Neurons at 14 different days *in vitro* (DIV) transfected with the enhanced green fluorescent protein (EGFP) plasmid were processed on 18 DIV for immunofluorescence staining and confocal imaging as previously described (Chao et al., 2012). The images were quantified using the MetaMorph software and then exported into Excel and GraphPad Prism for the analyses. Approximately 3000 spines within 20 μm dendritic segments 30 μm away from the somas of 30 neurons were measured in each group (Chao et al., 2008).

Synaptosome, synaptic density, and synaptic cytosol preparation

The cortices and hippocampi rapidly removed from the 3-month-old male mouse were homogenized in 2 ml sucrose buffer (10 mM HEPES, pH 7.5, 1.5 mM $MgCl_2$, 320 mM sucrose, 5 mM EDTA, 5 mM dithiothreitol (DTT), 0.1 mM PMSF, 10 μM MG132, and 1X protease and phosphatase inhibitors). Homogenates were centrifuged at 700 $\times$ *g* for 10 min at 4°C to remove nuclei and cell debris. The supernatant was then centrifuged again at 9250 $\times$ *g* for 15 min to obtain the pellet containing the crude synaptosome. The crude synaptosome fraction was resuspended in sucrose buffer with 1% Triton X-100 at 4°C for 60 min, followed by 40,000 $\times$ *g* centrifugation for 30 min to obtain the pellet (synaptic density) and supernatant (synaptic cytosol).

RNA immunoprecipitation and quantitative PCR

Cerebral cortices isolated from 3-month-old male mice were homogenized in 2 ml of RNA immunoprecipitation (RIP) buffer (DEPC-treated water containing 20 mM HEPES, pH 7.4, 150 mM NaCl, 1 mM $MgCl_2$, 0.5% Triton X-100, 0.5% NP-40, 10% glycerol, 0.5 mM DTT, 1X protease inhibitor cocktail, and 40 U/ml RNase inhibitor), and incubated at 4°C for 60 min on a rotator. Insoluble debris was pelleted at 10,000 *g* for 5 min. The supernatant was divided and incubated with either control or CPEB3 IgG-bound beads for 3 h. The beads were washed with RIP buffer five times, and 1/5 of the bead volume was used for immunoblotting. The remaining beads were eluted with 4 M guanidine thiocyanate, followed by phenol/chloroform extraction and ethanol precipitation in the presence of 5 μg of glycogen. The RNA precipitates were reverse transcribed using oligo-dT and ImPromII Reverse Transcriptase (Promega). Quantitative PCR (qPCR) was conducted using the Universal Probe Library and Lightcycler 480 system (Roche). The data analysis was performed using the comparative C_t (threshold cycle value) method with the nonCPEB3-targeted RNA, GAPDH mRNA (total RNA and RIP experiments), or synaptophysin mRNA (polysome experiment) as the reference. The PCR primers used were as follows: PSD95, 5′-GGCGCA CAAGTTCATTGAG and 5′-TGAGACATCAAGGATGCAGTG; NR1, 5′-TACAAGCGACACAAGGATGC and 5′-TCAGTGGGATGGTACTGC TG; NR2A, 5′-CTGCTCCAGTTTGTTGGTGA and 5′-AGATGCCCGTAA GCCACA; NR2B, 5′-GGGTTACAACCGGTGCCTA and 5′-CTTTGCCG ATGGTGAAAGAT; GluA1, 5′-CGGAAATTGCTTATGGGACA and 5′-AC ACAGCGATTTTAGACCTCCT; GAPDH, 5′-GCCAAAAGGGTCATCA

TCTC-3′ and 5′-CACACCCATCACAAACATGG-3′; synaptophysin, 5′-CAAGGCTACGGCCAACAG-3′ and 5′-GTCTTCGTGGGCTTCACTG-3′.

Sucrose density gradient for polysomal profiling

Two plates of WT or KO cortical neuron cultures at 18 DIV (~10^7 neurons) were washed with PBS, lysed in 600 μl buffer (25 mM HEPES, pH 7.5, 100 mM NaCl, 10 mM $MgCl_2$, 100 μg/ml cycloheximide, 0.25 M sucrose, 40 u/ml RNase inhibitor, and 1X protease inhibitor cocktail), and centrifuged for 5 min at 10,000 *g* at 4°C. Approximately 500 μl of supernatant was layered on top of a linear 15%–50% (w/v) sucrose gradient. Centrifugation was performed in a SW41 rotor at 37,000 rpm for 2 h. Polysome profiles were monitored by absorbance of light with a wavelength of 254 nm (A_{254}).

RNA extraction, Northern blotting, and RT-PCR

Sucrose gradient fractions were treated with 100 μg/ml Proteinase K and 0.2% SDS for 20 min at 37°C, phenol/chloroform extracted and precipitated with isopropanol to obtain RNAs. Total RNA was extracted using Trizol reagent (Invitrogen). Thirty micrograms total RNA isolated from WT, heterozygous, and KO tissues was used for Northern blotting. A 285 bp CPEB3 cDNA region, amplified using the sense exon3, 5′-GGTAAACACTACCCTCCC-3′, and the antisense exon6, 5′-CACCTTTCTAGAGTAGCGTTC-3′ primers, was used to synthesize the radiolabeled probe by random primer labeling. The cDNAs reverse transcribed from brain and testis RNAs were used for PCR with the sense primer exon2, 5′-ATGGAGGATAACGCTTTCCG-3′, exon3 or exon7, 5′-ACTGCCAGCTTTCGCAGG-3′ along with the antisense primer exon11, 5′-TACTGCAGACAGGTGACG-3′.

Plasmid construction, in vitro *transcription, and luciferase reporter assay*

Mouse PSD95 3′-UTR was PCR-amplified from brain cDNA using the primers 5′-CGGAATTCTTCCTGCCCTGGCTTGGCC-3′ and 5′-CCGCTCGAGCAAGTGTCTGTCTCTTCCTTTC-3′. The DNA fragment was cloned into the pcDNA3.1 and pcDNA3.1-FLuc plasmid. The RNAs used for transfection were synthesized using the mMessage mMachine T3 and T7 Ultra kits (Invitrogen). Hippocampal neurons at 10–11 DIV were cotransfected with 1.1 μg EGFP, myc-CPEB3, or myc-CPEB3C RNA along with 0.2 μg of firefly luciferase RNA appended to the PSD95 3′-UTR and 0.05 μg of *Renilla* luciferase RNA using the TransMessenger Transfection reagent (Qiagen). Six hours after transfection, the neurons were harvested for the dual luciferase assay (Promega).

Behavior assays

Open field. Each male mouse was released into a corner of the arena and allowed to explore for 60 min. The recorded moving trace of each mouse was analyzed using the TopScan system (Clever Sys).

Elevated plus maze. The elevated plus maze (EPM) consisted of two open arms with 1 cm ledges and two enclosed arms with 15 cm walls. The maze was elevated to a height of 50 cm above the floor during the task. The mouse behaviors were recorded in a 5 min testing period and analyzed using the TopScan system.

Rotarod. The male mice were placed on rotating drums with gradually accelerated speeds from 0 to 40 rpm. The time each mouse was able to maintain its balance on the rod and the minimum speed at which the mice would fall were recorded.

Shock activity. To measure the sensory and pain thresholds in mice, the male mice were given a 1 s shock with increasing intensity from 0.05 mA to 0.4 mA at a 0.05 mA interval until the mice became aware, vocalized, or jumped in response to the shock (Irvine et al., 2011).

Contextual fear conditioning. A chamber with an electrified floor grid and a video camera (Clever Sys FreezeScan) was used to measure the freezing response in mice. On the day of fear conditioning, the male mice were placed in the chamber, and a 2 s 0.5 mA foot shock was given every 2 min for four times. The mice were then placed back into their cages 2 min after the final shock. Extinction trials were followed 24 h later in the same chamber.

Morris water maze. The male mice were trained in a circular pool filled with milky water, which was maintained at 20°C (Morris, 1984). A circular platform was placed 1 cm beneath the water surface in the center of one quadrant. Training for the hidden platform version of Morris water maze (MWZ) consisted of four trials each day for 4 consecutive days. The probe trial was administered 24 h after the four training days. During the reversal training, the acquisition training of the new platform position consisted of four trials for 1 d, followed by a probe test 24 h later. The reversal learning was repeated two more times. Last, the escape platform, which was marked by a visible flag, was placed to ensure the swimming ability and visual acuity of the mice. For all of the trials, the maximal swimming duration was 60 s and the intertrial interval (ITI) was 15 min. The trajectories of the mice were recorded and analyzed using the video tracking and measuring system, TrackMot (Singa Technology). All of the behavioral data were analyzed using STATISTICA software. Student's *t* test, one-way ANOVA, two-way ANOVA, and Fisher's LSD *post hoc* test were used to determine the statistical differences.

Slice preparation and field recording

A male mouse was decapitated and the brain was immediately isolated and placed in ice-cold artificial CSF (aCSF), containing the following (in mM): 124 NaCl, 4.4 KCl, 1 NaH_2PO_4, 1.3 $MgSO_4$, 10 D-glucose, 26 $NaHCO_3$, 2.5 $CaCl_2$, and 0.5 ascorbic acid, pH 7.4, and oxygenated with 95% O_2 and 5% CO_2. Transverse hippocampal slices (400 μm thick) were prepared using a microslicer and recovered in a submerged holding chamber perfused with oxygenated aCSF at 28°C for at least 2 h. The slice was then transferred to an immersion-type chamber perfused with aCSF at a flow rate of 2–3 ml/min and maintained at 30 ± 1°C to record the field EPSP (fEPSP). A concentric bipolar tungsten stimulating electrode (No. 795500; A-M Systems) was placed in the stratum radiatum near the CA2 region and a glass recording microelectrode (No. 615500; A-M Systems) filled with aCSF was placed in the stratum radiatum of the CA1 region. The input–output responses were measured using the stimulus intensity from 20 to 110 μA. PPF was measured at interpulse interval (IPI) from 10 to 250 ms. Baseline stimulation (0.017 Hz, 0.1 ms pulse duration, biphasic) was adjusted to evoke 30–40% and 50% of the maximal response for long-term potentiation (LTP) and LTD, respectively. The quantification of synaptic transmission strength was measured using the slope of fEPSP (using the minimum slope from 10 to 90% of the rising phase). A stable baseline was acquired 20–30 min before stimulation. LTD was induced by LFS (1 Hz 15 min) or PP-LFS (50 ms IPI, 1 Hz 15 min). Long-term potentiation (LTP) was evoked by high-frequency stimulation (HFS): one train of 100 Hz, two trains of 100 Hz (20 s ITI), four trains of 100 Hz (5 min ITI), one train of theta-burst stimulation (TBS; nine bursts of four pulses at 100 Hz, 200 ms interburst interval) or four trains of TBS (5 min ITI). The average fEPSP slope measured at the indicated time after stimulation was used for statistical comparisons by Student's *t* test.

Results

Generation of CPEB3-deficient mice

To investigate the role of CPEB3 in learning and memory, we used the cre-loxP strategy to generate CPEB3 KO mice in a C57BL/6 genetic background (Fig. 1*A*). The targeting vector was electroporated into C57BL/6 embryonic stem (ES) cells. Four correct targeting ES clones were injected into C57BL/6-Tyrc-2J (c2J) blastocysts for chimera production, where one of the injected blastocysts successfully produced germline-transmitted chimeras. After multiple crossings with C57BL/6 mice, C57BL/6 mouse lines expressing ubiquitous Flp recombinase or sperm-specific Cre recombinase to obtain CPEB3 heterozygous mice (Fig. 1*A*), the littermates from these heterozygous matings were used for all of the experiments in this study. When exon 2 was deleted, alternative usage of the first methionine codon in exon 3 resulted in premature termination. Using a probe against the exon 3–6 region, we found the presence of a truncated CPEB3 RNA in the heterozygous and KO tissues (Fig. 1*B*), suggesting that the premature stop codon in the truncated transcript did not efficiently trigger non-sense-mediated RNA decay (NMD) (Schoenberg and Maquat, 2012). The shorter CPEB3 transcript in the testis is caused by alternative polyadenylation (Morgan et

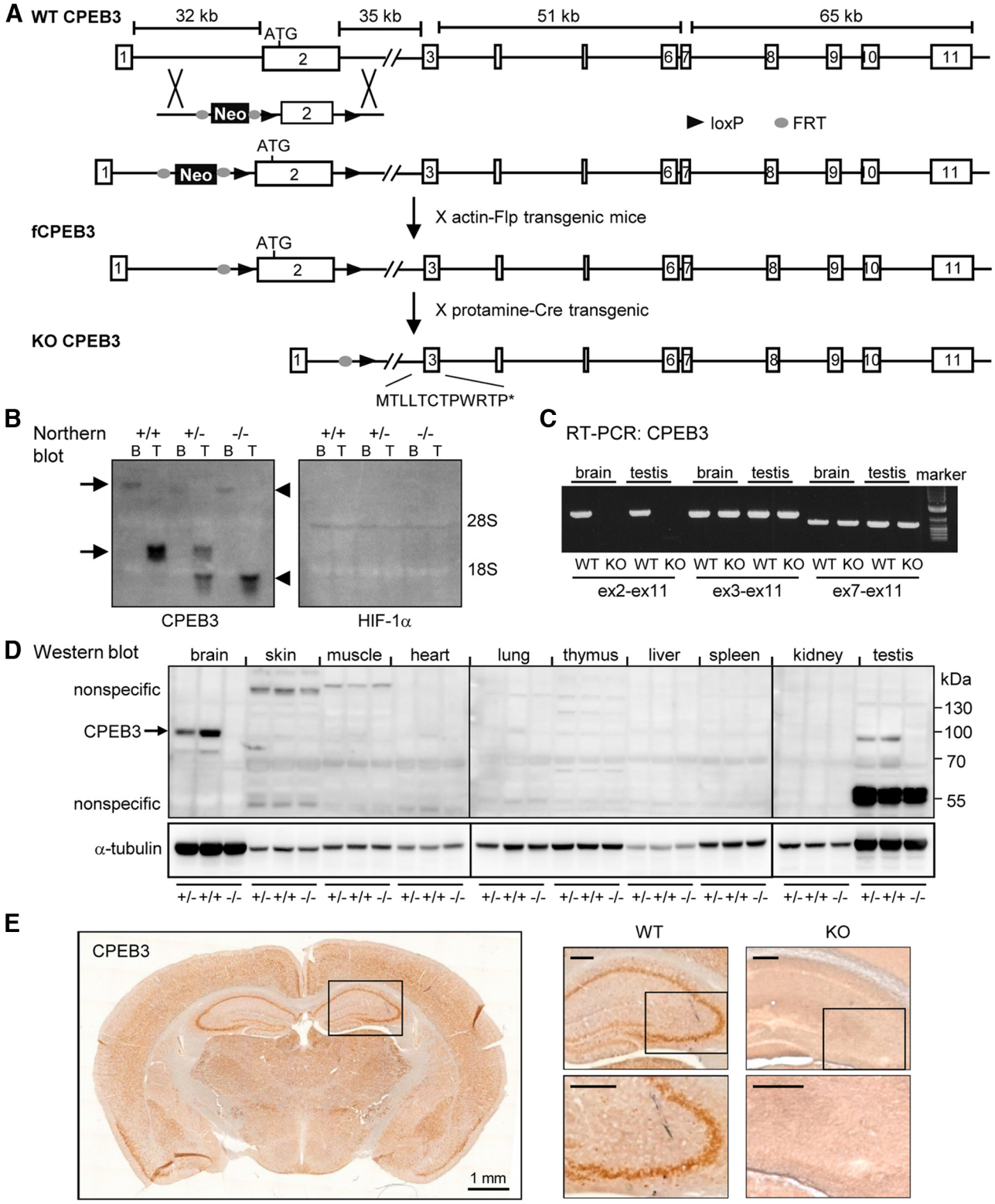

Figure 1. Generation and characterization of CPEB3-null mice. ***A***, ***B***, Schematic illustration of the targeting strategy. The *cpeb3* gene consists of 11 exons (numbered boxes) and spans a region of 185 kb. The targeting vector containing the flip recombinase target (FRT)-flanked phosphoglycerate kinase (PGK) promoter-driven neomycin-resistance gene (Neo) and loxP-flanked exon 2 cassette was inserted into the *cpeb3* gene by homologous recombination. After the excision of the PGK-Neo cassette by crossing with a C57BL/6 mouse line expressing Flp recombinase driven by a ubiquitous β-actin promoter (actin-flp), the resulting female progenies carrying the floxed CPEB3 allele CPEB3 (fCPEB3) were mated with C57BL/6 males containing a Cre recombinase transgene under the control of protamine promoter (protamine-cre) to excise exon 2 in sperms to produce the KO allele. Male offspring carrying WT (+/+), heterozygous (+/−) or KO (−/−) alleles from heterozygous matings were selected for (***B***) Northern blot analysis using a probe against exon 3–6 of CPEB3 RNA or HIF-1α RNA (loading control). The arrows denote two CPEB3 transcripts derived from alternative usage of the polyadenylation signals in the 3′-UTR. The arrowheads denote the truncated CPEB3 transcripts without the exon 2 sequence. ***C***, RT-PCR analysis using RNAs isolated from the brain and testes of WT and KO littermates confirmed the presence of exon 2-deleted CPEB3 transcript in the KO tissues. ***D***, ***E***, Western blotting (***D***) and immunohistochemistry (***E***) of coronal brain slices using the affinity-purified polyclonal CPEB3 antibody revealed no immunostained signal in the KO tissue. Scale bar, 0.25 mm unless specified.

Table 1. Home-cage monitoring

	CPEB3 WT ($n = 6$)		CPEB3 KO ($n = 6$)	
Time percentage	Day	Night	Day	Night
Awakening	0.017 ± 0.001	0.011 ± 0.001	0.016 ± 0.002	0.011 ± 0.001
Drinking	0.025 ± 0.018	0.852 ± 0.112	0.160 ± 0.019	1.180 ± 0.078
Feeding	1.779 ± 0.167	8.324 ± 0.498	1.884 ± 0.337	7.322 ± 0.755
Grooming	6.072 ± 0.498	11.12 ± 0.428	6.292 ± 0.581	12.04 ± 0.425
Hanging	0.468 ± 0.139	5.460 ± 0.852	0.154 ± 0.070	3.803 ± 0.724
Rearing	0.188 ± 0.060	0.848 ± 0.149	0.101 ± 0.021	0.781 ± 0.114
Resting	43.380 ± 0.778	19.16 ± 1.247	44.43 ± 1.104	18.72 ± 1.609
Twitching	0.407 ± 0.049	0.211 ± 0.020	0.388 ± 0.025	0.209 ± 0.029
Walking	0.418 ± 0.061	1.244 ± 0.131	0.619 ± 0.134	1.886 ± 0.222
Travel distance (cm)	87.322 ± 11.82	369.07 ± 46.78	104.87 ± 16.65	435.96 ± 63.84

al., 2010). Using the more sensitive assay, RT-PCR, we confirmed the absence of exon 2 in CPEB3 RNA in the KO tissues (Fig. 1*C*). Moreover, no CPEB3 protein was detected in the KO tissues using Western blotting (Fig. 1*D*) and immunohistochemistry assay (Fig. 1*E*) with the affinity-purified polyclonal CPEB3 antibody. Thus, we produced a mouse line deficient in CPEB3 protein.

CPEB3 KO mice showed higher anxiety in the open field and elevated short-term fear response in the contextual fear conditioning

The following behavior studies were blindly conducted to the genotypes using 2- to 3-month-old male WT and KO littermates. The body weight (WT: 22.84 ± 0.4 g; KO: 22.58 ± 0.5 g, $n = 40$), home-cage behaviors (Table 1), and physical performance assessed using the modified SmithKline/Harwell/Imperial College/Royal Hospital/Phenotype Assessment (SHIRPA) procedures (Masuya et al., 2005, Table 2) were similar between the two groups of mice. Anxiety-like responses and exploratory behaviors were studied in the open field and EPM. Normally, mice fear an open environment and tend to avoid the center of the field or the elevated open arm. The extent of anxiety is determined by counting the number of entries and the duration of stay by the test animal into the center zone in the open field (Fig. 2*A*,*B*) or into the open arm in the EPM (Fig. 2*C*). The KO mice showed elevated anxiety in the open field, but not the EPM because they spent less time and showed a reduced number of crosses into the center arena (Fig. 2*A*). Although the locomotor activity of the null mice was significantly lower (i.e., total distance) in the open field, the KO mice preferred to not enter the center even after taking this factor into consideration (Fig. 2*B*). The reduced locomotor activity in the open field was not due to motor problems given that the KO mice showed normal motor coordination on the rotarod (Fig. 2*D*) and demonstrated similar locomotor abilities to WT littermates in the home-cage environment (Table 1).

We next used contextual fear conditioning and MWZ to examine hippocampus-dependent memory. In the former assay, the mice learned to express a fear response (i.e., freezing) when faced with a conditioned stimulus (CS, the chamber environment), which was previously paired with a noxious unconditioned stimulus (US, electrical foot shock). In contrast, if the mice were exposed only to the CS without US pairing, then previously acquired fear responses would gradually decline. This process is known as extinction. The freezing levels in WT and KO mice were similar during habituation, increased significantly after CS–US paired trainings (i.e., acquisition, $F_{(4,72)} = 115.57$, $p < 0.001$), and were significantly reduced during extinction ($F_{(4,72)} = 18.998$, $p < 0.001$), indicating that both groups of mice could perform associated learning tasks (Fig. 2*E*). Importantly, the KO group learned more rapidly during acquisition ($F_{(1,18)} = 4.9791$, $p < 0.05$), but slower during extinction ($F_{(1,18)} = 20.4272$, $p < 0.001$). *Post hoc* comparisons revealed that the KO mice showed increased freezing in the second and third trials during acquisition ($p < 0.05$) and extinction ($p < 0.01$). Nevertheless, given sufficient training, the consolidated long-term fear memory and extinction memory, as determined 1 d after acquisition (i.e., the freezing response in the first extinction trial) and recalled 7 d after extinction, respectively, were normal in the KO mice (Fig. 2*E*). The average current intensities required to trigger a specific response, awareness, vocalization, or jumping in WT and KO mice were similar (Fig. 2*F*), suggesting that the KO animals displayed a normal perception of shock.

CPEB3 KO mice had enhanced consolidated spatial memory in the MWZ

During spatial acquisition, the mice learned to locate a hidden platform using visual cues around the maze. Both WT and KO mice learned where the platform was positioned as evidenced by the decreasing latencies over the 4 d training period ($F_{(3,42)} = 68.2152$, $p < 0.001$); however, no difference in spatial learning between groups was observed ($F_{(1,14)} = 2.744$, $p = 0.1198$; Fig. 3*A*). During the probe trial, the hidden platform was removed and the amount of time that the mice spent in the target quadrant, where the platform was previously placed, was recorded to determine their consolidated LTM. Both WT and KO mice spent a significant time in the target quadrant (WT: $F_{(3,28)} = 5.1255$, $p < 0.001$; KO: $F_{(3,28)} = 50.208$, $p < 0.001$). Moreover, the KO mice showed better consolidated spatial memory because they spent more time in the target quadrant relative to their WT littermates ($F_{(1,7)} = 1.797$, $p < 0.05$, Student's t test; Fig. 3*B*). During the reversal trials (Fig. 3*C*), the hidden platform was moved to a different quadrant and the mice learned to locate the platform in its new position for 1 d of the four spatial trainings. The probe test was followed 24 h later. Although there was no difference in reversal spatial learning between the two groups of animals (the latency to escape in seconds, on day 9, WT: 31.68 ± 7.98 vs KO: 29.19 ± 6.71; day 11, WT: 30.50 ± 10.76 vs KO: 28.63 ± 8.47; day 13, WT: 30.69 ± 10.42 vs KO: 33.94 ± 8.50), the KO mice clearly spent less time in the newly acquired Q4 quadrant compared with WT littermates in the first reversal probe test (Fig. 3*C*). Such a difference was likely caused by the stronger consolidated memory for the previous Q2 platform position in the KO mice (Fig. 3*B*). Both of the groups of mice navigated >25% of time in the Q2 quadrant in the first reversal probe trial, but soon learned to relocate the platform in the most recently trained quadrant in the second and third reversal probe tests (Fig. 3*C*). Last, using the visible platform, we ensured that the swimming ability and visual acuity of the KO mice were normal (Fig. 3*D*).

Enhanced PP-LFS-elicited LTD in juvenile CPEB3 KO mice

To examine whether specific forms of synaptic plasticity were altered in the SC-CA1 pathway of the KO hippocampus, we used hippocampal slices isolated from juvenile and adult mice for LTD and LTP studies. The basic synaptic responses, including the input–output relationship (Figs. 4*A*, 5*A*) and PPF (Figs. 4*B*, 5*B*), did not differ between the WT and KO groups. LTD induced by LFS was normal (Fig. 4*C*), but evoked by PP-LFS was enhanced in young KO hippocampal slices (Fig. 4*D*). PP-LFS-evoked LTD required the activation of NMDARs in 3- to 4-week-old WT and KO mice (Fig. 4*D*). PP-LFS is a stronger induction protocol, which can also evoke NMDAR-independent LTD in adult mice (Oliet et al., 1997; Kemp et al., 2000). However, no difference was found in this form of LTD if adult slices were used (Fig. 5*C*).

Table 2. SHIRPA modified assays

	CPEB3 WT ($n = 6$)	CPEB3 KO ($n = 6$)
I. In the viewing jar		
Coat color	Normal	Normal
Hair length	Normal	Normal
Hair morphology	Normal	Normal
Respiration rate	Normal	Normal
Tremor	No shaking	No shaking
Body position	Sitting or standing	Sitting or standing
Spontaneous activity	Vigorous scratching, grooming, moderate movement	Vigorous scratching, grooming, moderate movement
Defecation, no of feces	2	1
II. In the arena		
Urination	No	No
Time elapsed before the mouse starts to move, seconds	2.5 ± 0.29	3.75 ± 0.85
Locomotor activity, no. of squares	22 ± 3	21 ± 4
Transfer arousal	Brief freeze, then active movement	Brief freeze, then active movement
Piloerection	None	None
Palpebral closure	Both eyes wide open	Both eyes wide open
Startle response	Preyer reflex	Preyer reflex
Gait	Normal	Normal
Pelvic elevation	Elevated	Elevated
Tail elevation	Extended horizontally	Extended horizontally
Touch escape	Vigorous	Moderate
III. Above arena		
Positional passivity	Struggles when held by tail	Struggles when held by tail
Trunk curl	Absent	Absent
Limb grasping	Absent	Absent
Visual placing	Upon vibrissa contact	Upon vibrissa contact
Grip strength	Slight grip	Slight grip
Body tone	Slight resistance	Slight resistance
Head morph	Normal	Normal
Pinna reflex	Active retraction, moderately brisk flick	Active retraction, moderately brisk flick
Pinna morph, R	Normal	Normal
Pinna morph, L	Normal	Normal
Corneal reflex	Single blink	Single blink
Toe pinch	Brisk, rapid withdrawal	Brisk, rapid withdrawal
IV. On the arena		
Tail morphology	Normal	Normal
Lacrimation	None	None
Whisker morph	Normal	Normal
Teeth morph	Normal	Normal
Provoked biting	Present	Present
Salivation	Slight margin of the submaxillary area	Slight margin of the submaxillary area
Heart rate	Normal	Normal
Abdominal tone	Slight resistance	Slight resistance
Skin color	Pink	Pink
Limb morph FR	Normal	Normal
Limb morph FL	Normal	Normal
Limb morph HR	Normal	Normal
Limb morph HL	Normal	Normal
Limb tone	Slight resistance	Slight resistance
V. In the arena, part 2		
Wire maneuver	Unable to grip with a hindlimb	Unable to grip with a hindlimb
Righting reflex	No impairment	No impairment
Contact righting reflex	Tries	Tries
Negative geotaxis	Moves, but fails to turn	Moves, but fails to turn
VI. Additional comments		
Fear	Does not freeze	Does not freeze
Irritability	Does not violently struggle	Does not violently struggle
Aggression	No	No
Vocalization	Yes	Yes
Bizarre behavior	No bizarre behavior	No bizarre behavior
Convulsion	No phenotype	No phenotype

Adult KO hippocampal slices were analyzed for potential deficits in LTP elicited by one, two, or four trains of HFS, or one or four trains of TBS (Patterson et al., 2001; Alarcon et al., 2004). All forms of LTP were normal in the KO slices (Fig. 5*D–H*), even though the CPEB3-null mice displayed better spatial memory (Fig. 3). Numerous studies using pharmacological or genetic manipulations have demonstrated that the causal relation between LTP/LTD and phenotypic changes in LTM does not always exist. For example, LTP is viewed as a long-lasting enhancement in synaptic efficacy following stimulation. Nevertheless, the mice expressing a mutant PSD95 had potentiated LTP and absence of LTD, yet exhibited impaired spatial memory in the MWZ (Migaud et al., 1998). From the field-recording data, we found that ablation of the *cpeb3* gene facilitated a specific form of long-term plasticity, PP-LFS-induced LTD, at the SC-CA1 synapses of juvenile (i.e., NMDAR-dependent) but not adult (i.e., NMDAR-independent) KO slices.

Dendritic spine enlargement in CPEB3 KO neurons

Behavioral and electrophysiological studies indicated that the KO mice had aberrant memory and plasticity relative to their WT littermates. To investigate the molecular and cellular defects caused by CPEB3 depletion, we used cortical/hippocampal tissues isolated from WT and KO E18 embryos for neuronal cultures. Because female KO mice exhibited severely reduced fertility, the embryos of different genotypes were collected from heterozygous matings and showed no significant difference in their body weights (Fig. 6*A*). The spine morphology of WT and KO pyramidal excitatory neurons was analyzed. Neurons (14 DIV) transfected with a plasmid expressing EGFP were fixed for immunostaining at 18 DIV to clearly outline the morphology of transfected neurons. Overall, depletion of CPEB3 did not affect the gross morphology of neurons (Fig. 6*B*). However, when compared with WT neurons at higher magnification, the width of the spine head (but not the density and length of the spine) in KO neurons was significantly increased (Fig. 6*B*, *C*).

Elevated surface expression of NMDARs in CPEB3 KO neurons

Because the KO pyramidal neurons showed normal dendritic arborization but enlarged spine morphology, we followed the expressions of CPEB3 and several glutamatergic synapse molecules during neuronal development in culture. The lysates harvested from WT and KO neurons of different DIV were used for immunoblotting. The CPEB3 level was low at the early stages during axonal and dendritic growth, and plateaued after 2 weeks in culture. Importantly, the expression levels of several PRPs, such as the subunit of NMDAR, NR1, the subunit of AMPAR, GluA1, and PSD95, began to increase in 15–19 DIV KO neurons (Fig. 7*A*). Although GluA1 was previously reported target of CPEB3, it is not known that the lack of CPEB3 in neurons can

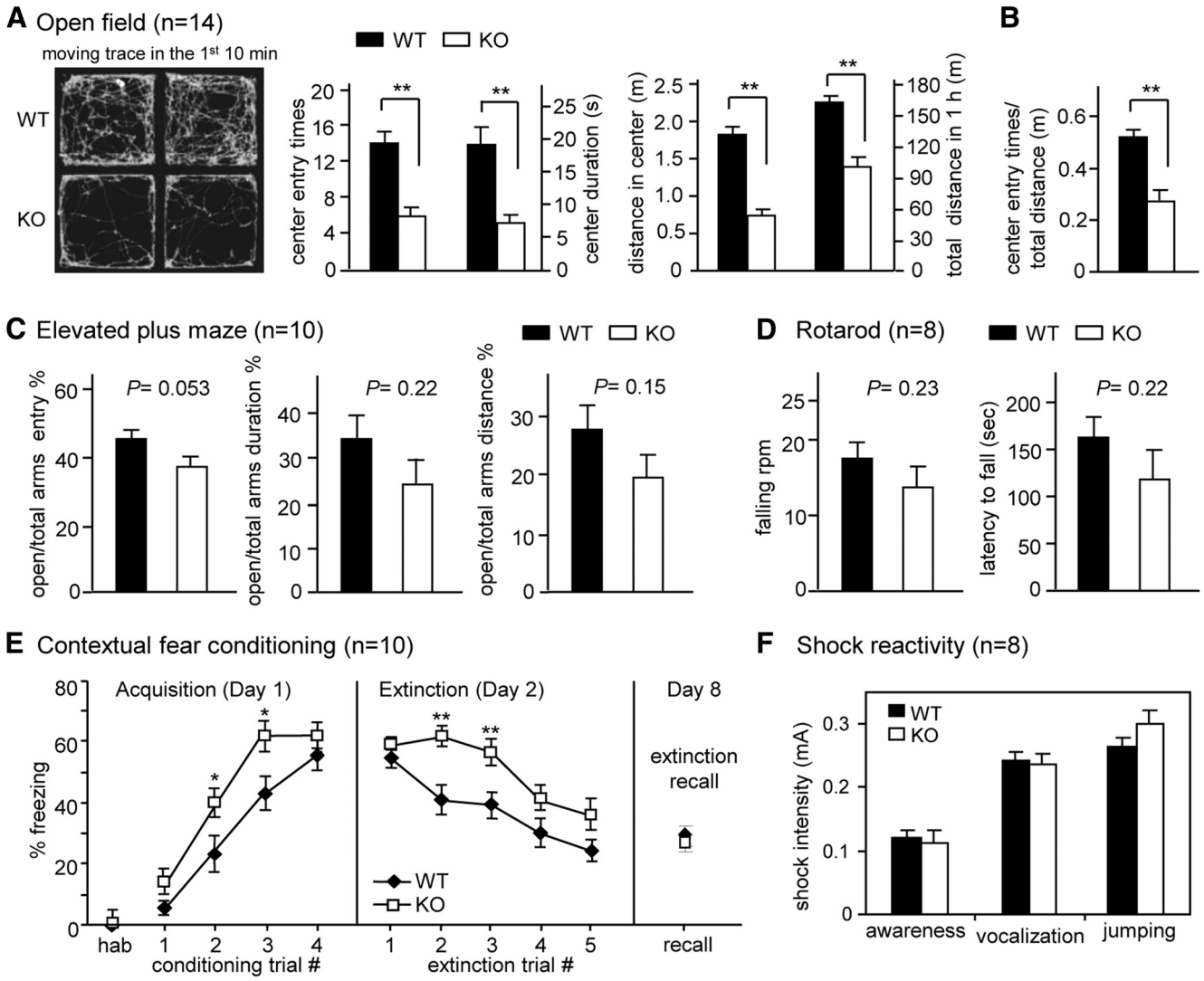

Figure 2. Behavioral characterization. Anxiety level and exploratory behavior of WT and KO mice were assessed using open field and EPM tasks. ***A***, Representative moving traces in the open arena are shown. The entry times, staying duration, and traveling distance in the center during the first 10 min and the total 1 h moving distance in the arena were presented as bar graphs. ***B***, The center entry times were normalized against the moving distance in the first 10 min. ***C***, The percentage of entry and staying duration into the open arms versus the total arms in the EPM was analyzed. ***D***, Rotarod. The rotating speed that caused the mouse to fall and the latency in which the mouse could stay on the rotating rod were analyzed. ***E***, Contextual fear conditioning. The freezing response during habituation (hab) and acquisition was analyzed for 2 min per trial. A foot shock was given at the end of habituation and the first three conditioning trials. During extinction, the mouse was placed in the chamber for 30 min without reinforcing the shock. The freezing level was analyzed every 6 min for five segments. Consolidated extinction memory was recalled a week later by monitoring the freezing behavior for 6 min in the original chamber. ***F***, Shock reactivity. The current intensities required to evoke various responses in the mice were recorded. The data were expressed as mean ± SEM; $*p < 0.05$ and $**p < 0.01$, Student's *t* test.

result in elevated expression of PSD95 and the essential NMDAR subunit, NR1 (now known as GluN1). To further examine this phenomenon, we examined calcium influx $[Ca^{2+}]_i$ through the opening of NMDARs in Fura2-AM-filled WT and KO neurons using ratio-matrix analysis (F/F_0). The increased $[Ca^{2+}]_i$ induced by exposure to NMDA was higher in KO neurons (Fig. 7*B*, peak). This NMDA-induced $[Ca^{2+}]_i$ could be suppressed by the copresence of a high extracellular concentration of the NMDAR blocker, Mg^{2+}. Furthermore, such a defect could be rescued by ectopically expressing myc-CPEB3 (Fig. 7*B*, blue line and bars), suggesting that elevated NMDAR-induced $[Ca^{2+}]_i$ was unlikely caused by other compensatory mechanisms in the absence of CPEB3. As CPEB3 is a translational repressor, we next examined whether total and synaptic NMDAR and PSD95 remained upregulated in the KO adult brain. The NMDAR is a heterotetrameric complex composed of two obligatory NR1 subunits and two NR2(A–D) subunits and/or more rarely, NR3 subunits (Cull-Candy et al., 2001). Because the prevalent NR2 subunits in adult forebrain are NR2A and NR2B (now known as Grin2A and Grin2B), brains isolated from the 3-month-old mice were biochemically fractionated to obtain synaptic density and synaptic cytosol for immunodetection of GluA1, PSD95, and the predominant NMDAR subunits (NR1, NR2A, and NR2B) (Fig. 8*A*). Both the total and synaptic levels of PSD95, NR1, NR2A, and NR2B were elevated in CPEB3-deficient brains (Fig. 8*A*, bar graphs). Moreover, GluA1, the previously identified CPEB3 target (Pavlopoulos et al., 2011), was slightly upregulated in the total lysate and synaptic density, but more upregulated in the synaptic cytosol. Alterations in these protein expressions occurred post-transcriptionally given that the amounts of these RNAs remained the same in the KO brains (Fig. 8*B*).

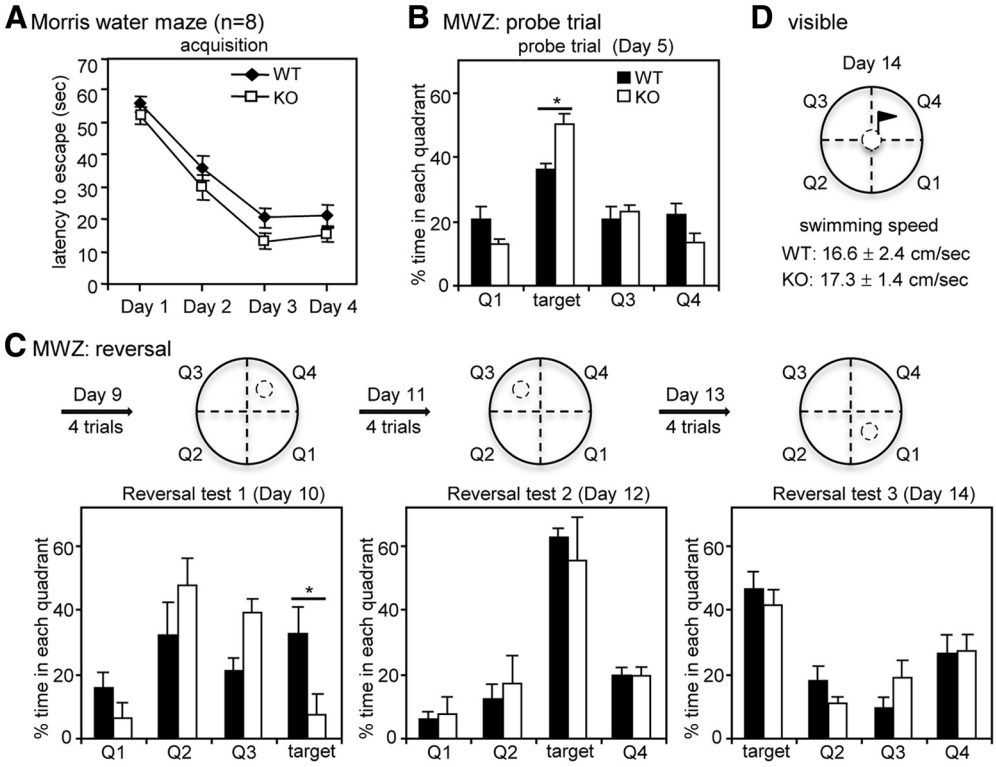

Figure 3. CPEB3 KO mice showed enhanced consolidated spatial memory in the MWZ test. ***A***, The WT and KO mice normally learned in the hidden platform version of MWZ within four trials per day for 4 consecutive days. ***B***, In the probe trial, the platform was removed, and the percentage of time that the mouse spent navigating in each quadrant was analyzed. Both of the groups of mice searched closer to the target quadrant where the platform had been previously placed. ***C***, Reversal learning. On day 9, the mice were trained for four trials to locate the hidden platform in a new position. The reversal probe test was conducted 24 h later on day 10. The reversal learning and probe test were repeated two more times with an altered platform position. ***D***, The motor ability and visual acuity of the mice were assessed by the swimming speed in the cued version of MWZ, in which the platform was indicated by a visible flag. All of the data were expressed as the mean ± SEM; $^*p < 0.05$ (Student's *t* test).

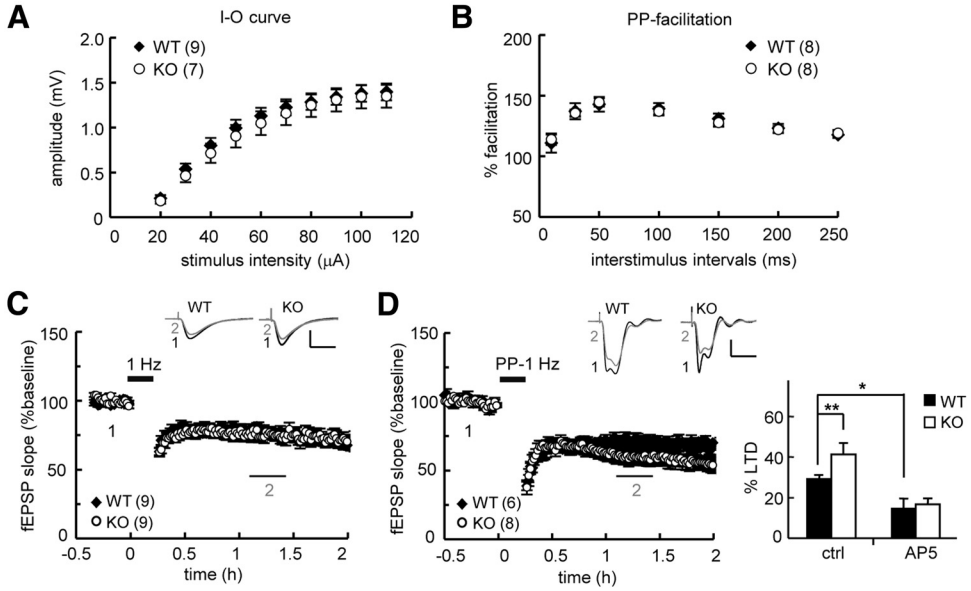

Figure 4. Genetic ablation of CPEB3-facilitated PP-LFS-induced LTD in the SC pathway of juvenile (3- to 4-week-old) hippocampal slices. Basal synaptic transmission. ***A***, ***B***, Input– output (I–O) curve and (***B***) paired-pulse (PP) facilitation did not show a significant difference between the WT and KO mice ($p = 0.66$ and 0.97, respectively, two-way ANOVA). ***C***, ***D***, Normal LFS-induced LTD (WT: 76.82 ± 2.84%; KO: 75.37 ± 3.94%, $p = 0.96$, Student's *t* test, at 50–70 min after stimulation) and (***D***) increased PP-LFS-elicited LTD in the KO hippocampal slices (WT: 70.34 ± 3.70%; KO: 59.81 ± 5.48%, $p < 0.01$, Student's *t* test, at 50–70 min after stimulation). PP-LFS-evoked LTD was blocked by the NMDAR antagonist, 50 μM AP5. Numbers in parentheses represent the number of slices isolated from 4 to 5 male mice that were used for recordings. All of the data were expressed as the mean ± SEM. Statistics from ***C*** to ***D*** were analyzed using Student's *t* test. Traces represent baseline (black line, 1) and 50–70 min after stimulation (gray line, 2). Calibration, 0.5 mV, 20 ms.

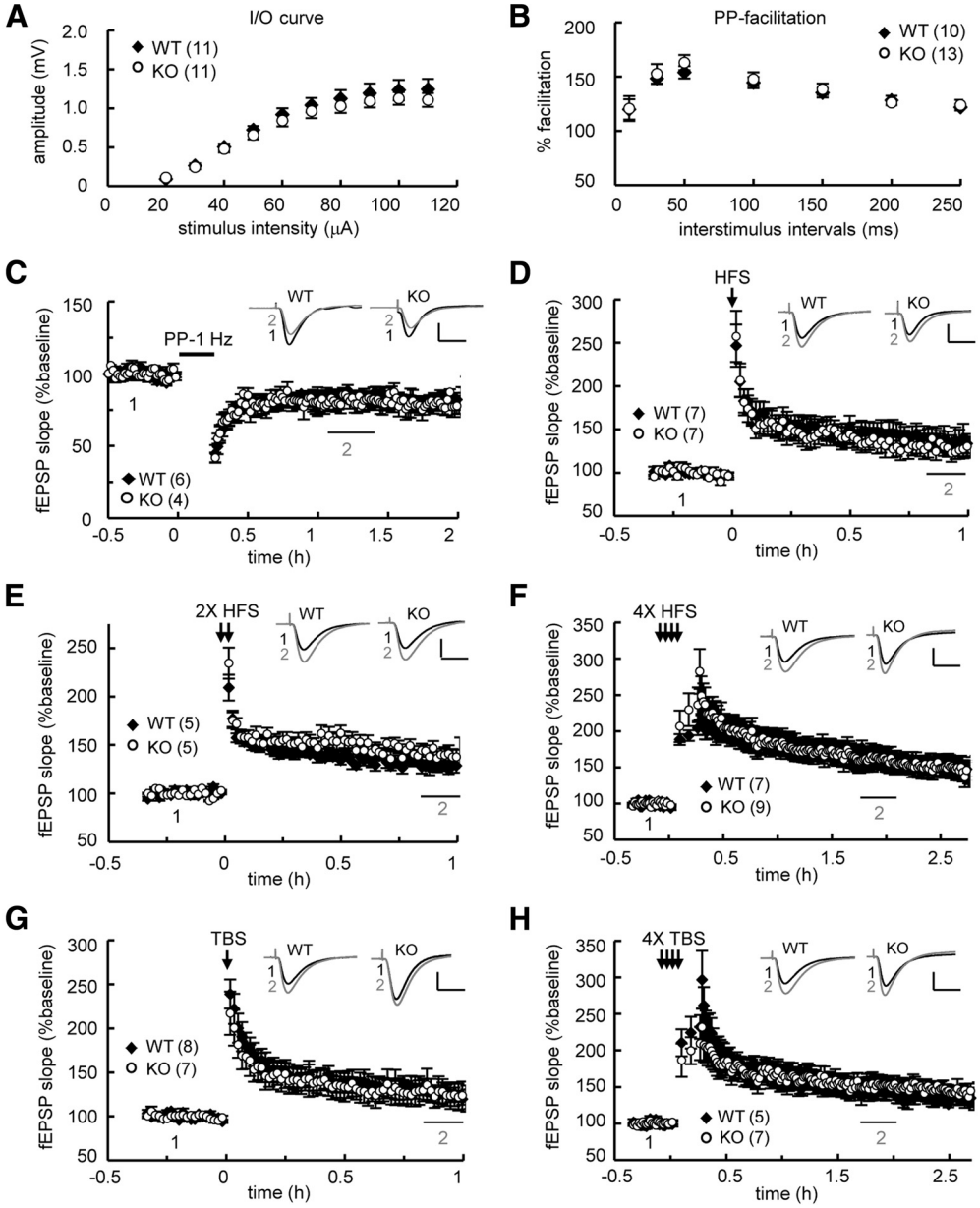

Figure 5. Normal LTP and LTD in the SC pathway of adult (9- to 12-week-old) KO hippocampal slices. Basal synaptic transmission. ***A***, ***B***, Input–output (I–O) curve and (***B***) paired-pulse (PP) facilitation were normal in the KO slices ($p = 0.09$ and 0.72, respectively, two-way ANOVA). ***C–H***, LTD induced by PP-LFS showed no significant difference (WT: 83.61 ± 3.71%, KO: 81.64 ± 4.74%, $p = 0.12$ at 50–70 min after stimulation) between the WT and KO groups. No significant difference was observed between the WT and KO slices in LTP evoked by (***D***) one train (1X) of HFS (WT: 136.67 ± 12.78%, KO: 128.77 ± 10.8%, $p = 0.10$ at 50–60 min), (***E***) two trains (2X) of HFS (WT: 128.6 ± 5.05%, KO: 126.39 ± 4.26%, $p = 0.43$ at 50–60 min), (***F***) four trains (4X) of HFS (WT: 165.84 ± 9.01%, KO: 162.8 ± 16.08%, $p = 0.43$ at 100–120 min after stimulation), (***G***) 1X TBS (WT: 126.07 ± 7.35%; KO, 126.32 ± 14.42%, $p = 0.96$ at 50–60 min), and (***H***) 4X TBS (WT: 145.42 ± 10.02%, KO: 151.42 ± 13.13%, $p = 0.08$ at 100–120 min after stimulation). Numbers in parentheses represent the number of recorded slices isolated from 4 to 5 male mice. All of the data were expressed as the mean ± SEM. Statistics from ***C*** to ***H*** were analyzed using Student's *t* test. Traces represent baseline (black line, 1) and the indicated time after stimulation (gray line, 2). Calibration: 0.5 mV, 20 ms.

PSD95 expression was translationally upregulated in CPEB3-deficient neurons

The elevated expression of NR1, NR2A, NR2B. and PSD95 at the protein level in CPEB3 KO brains could be directly caused by translational upregulation in the absence of the repressor, CPEB3 (Fig. 8). Thus, we tested whether CPEB3 could bind to these RNAs using RIP (Fig. 9*A*). Similar to the previously identified GluA1 RNA, there was a >2-fold increase in PSD95 and NR1 RNAs and ~1.5-fold increase in NR2A and NR2B RNAs, but not of the negative control glyceraldehyde 3-phosphate dehydrogenase (GAPDH) RNA pulled down in the CPEB3 immunoprecipitates (Fig. 9*A*). Next, we investigated the translational status of GluA1, NR1, NR2A, NR2B, PSD95, and GAPDH mRNAs by comparing polysomal distributions of these RNAs in WT and CPEB3 KO neurons. The RNA distribution in each fraction is expressed as the percentage of total. A depletion of CPEB3 did not alter general polysome profiles (Fig. 9*B*). Notably, there was a shift of PSD95, NR1, and NR2A RNAs and a subtle migration of GluA1and NR2B RNAs, but not the control, GAPDH RNA, toward heavier density fractions. This revealed an enhanced association between these PRP mRNAs and larger polysomes, indicating increased translation of these PRP mRNAs (Fig. 9*B*). A

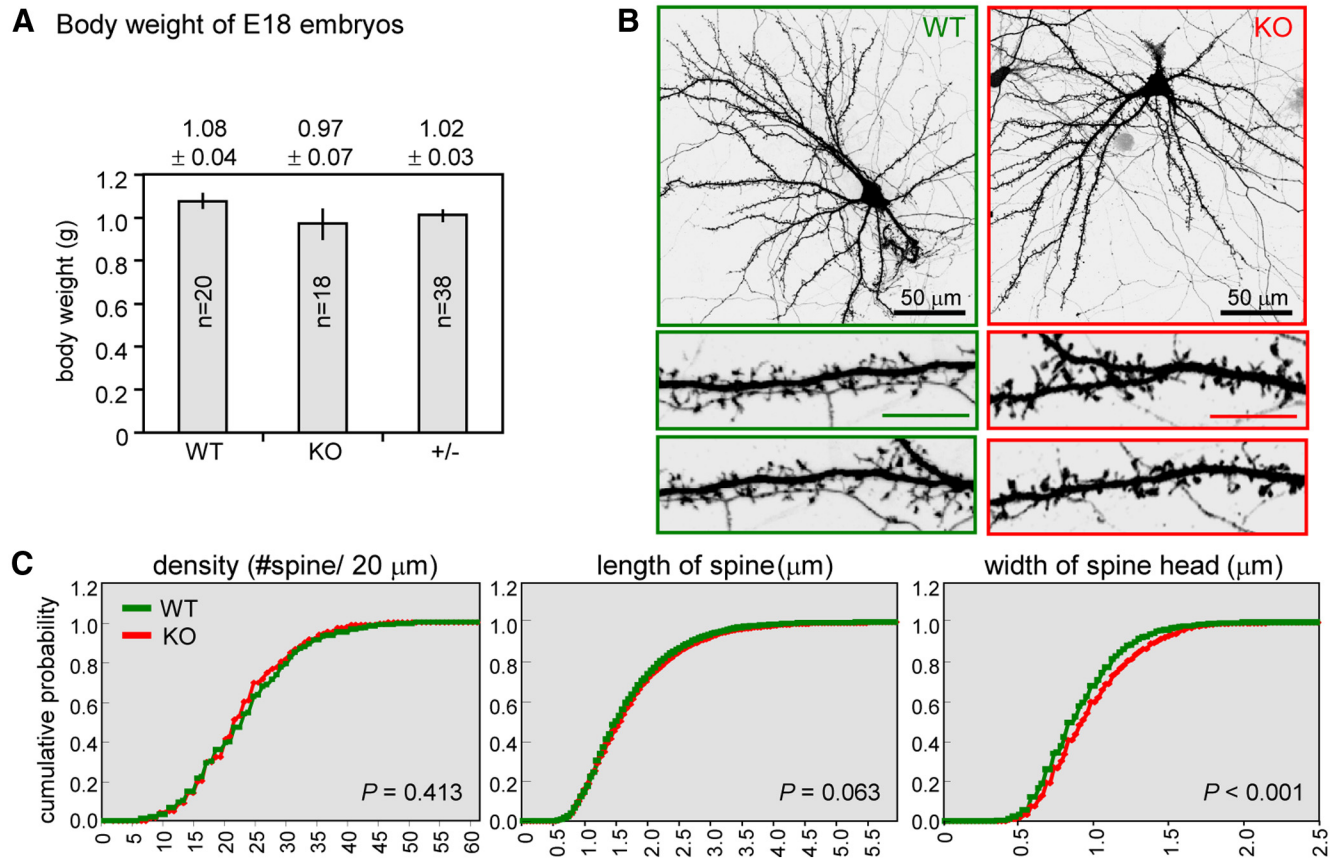

Figure 6. Enlarged dendritic spine heads in cultured CPEB3 KO neurons. ***A***, The body weight of E18 embryos isolated from heterozygous CPEB3 matings. ***B***, The WT and KO neurons were transfected with the GFP plasmid on 14 DIV and fixed on 18 DIV for GFP immunostaining. Representative images of the whole neurons and dendritic spine area are shown. Scale bars: 10 μm unless denoted. ***C***, Quantification analysis of dendritic spine morphology. Approximately 30 pyramidal neurons in each group (WT, green; KO, red) were collected from three independent cultures and analyzed using the MetaMorph software. The cumulative probability curves of density, length, and width of dendritic spines in each group (~3000 spines) were plotted and analyzed for the statistical difference between groups using Student's *t* test.

previous study has shown that association of NR2A (or NR2B) with PSD95 reduced the calpain-mediated cleavage of NR2A (or NR2B) in response to NMDA stimulation (Dong et al., 2004). Moreover, acute knockdown of PSD95 decreased AMPAR- and NMDAR-mediated EPSCs, although overexpression of PSD95 selectively potentiated AMPAR-mediated EPSCs in CA1 neurons (Ehrlich et al., 2007), suggesting that a change in PSD95 levels could regulate synaptic strength. Furthermore, we found that increased expression of PSD95 was observed 1–2 d earlier than GluA1 and NR1 (Fig. 7*A*) and that the 3′-UTR of PSD95 RNA was more complete compared with NR1, NR2A, and NR2B. Thus, we examined whether CPEB3 could directly bind to the PSD95 3′-UTR and repress translation of a reporter RNA appended to this sequence. The radiolabeled 3′UTRs of PSD95 and Arc (a negative control) mRNAs were subjected to *in vitro* UV-cross-linking with the C-terminal RBD of CPEB3 fused to maltose-binding protein (MBP-CPEB3C). The *in vitro* binding and RNA reporter assays revealed that CPEB3 directly bound to the 3′-UTR of PSD95 RNA (Fig. 9*C*) and suppressed 20–25% translation of the reporter RNA in neurons (Fig. 9*D*).

Discussion

This study demonstrates that CPEB3 functions as a negative regulator in learning and memory by confining the expression of several PRPs, including NR1, NR2A, NR2B, and PSD95. In conjunction with the previously identified CPEB3 targets, GluA1 and GluA2 RNAs (Huang et al., 2006; Pavlopoulos et al., 2011), CPEB3 coordinately constrained the syntheses of multiple PRPs that are critical for regulating the plasticity of glutamatergic synapses. Although CPEB3 was proposed to function as a translational activator once monoubiquitinated by Neurl1 (Pavlopoulos et al., 2011), it may not be the key substrate of Neurl1 that contributes to the better memory performance, facilitated LTP and LTD in Neurl1-overexpressing mice. That is because CPEB3 KOs also showed enhanced spatial memory and LTD. Crossing the Neurl1-transgenic mice with CPEB3 KOs will help clarify this issue. Genetically expressing a loss-of-function mutant, increasing or depleting the expression of NR1 (Tsien et al., 1996; Shimizu et al., 2000), NR2A (Cui et al., 2013), NR2B (Tang et al., 1999; von Engelhardt et al., 2008; Brigman et al., 2010), GluA1 (Chourbaji et al., 2008; Wiedholz et al., 2008), GluA2 (Jia et al., 1996), or PSD95 (Migaud et al., 1998; Beique et al., 2006) in mice results in various abnormalities in learning and memory. For example, GluR1 KO mice had hyper locomotor activity in the open field (Chourbaji et al., 2008) and NR2B transgenic mice showed enhancement in both consolidation and extinction of fear memory (Tang et al., 1999). When the translational repressor CPEB3 is genetically ablated, the expressions of these important glutamate signaling molecules are elevated, and at least in part, contribute to the abnormal spine morphology and aberrant behaviors observed in the KO mice. The molecular changes we identified so far may not explain all the behavioral differences

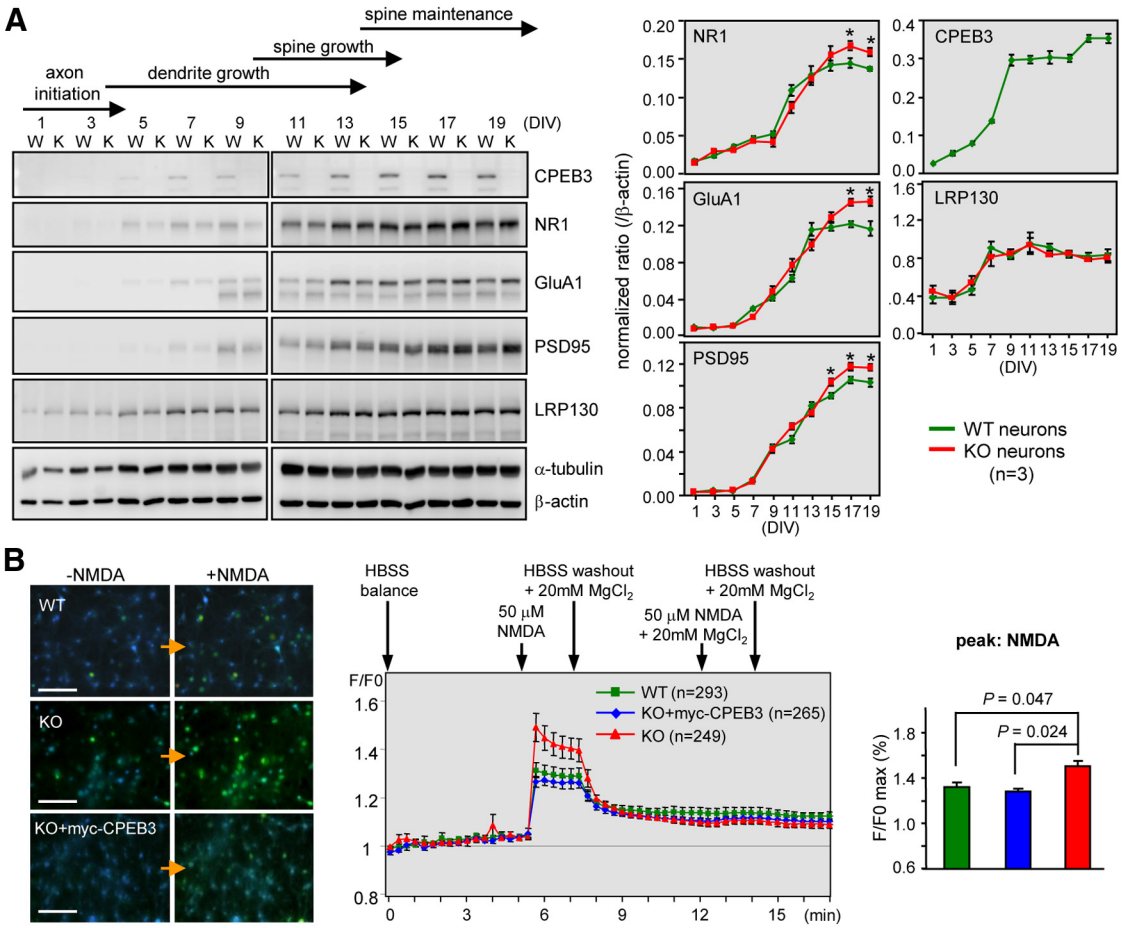

Figure 7. Elevated NMDAR-induced calcium influx in CPEB3 KO neurons. ***A***, Developmental expression of various synaptic proteins in WT and KO neurons. CPEB3 WT and KO neurons obtained at different DIV were harvested for Western blotting. The protein levels of NR1, GluA1, PSD95, CPEB3, and leucine-rich protein (LRP)130 were normalized against β-actin and plotted against DIV. The results from three independent cultures were quantified and displayed as the mean ± SEM. ***B***, WT and KO neurons at 16–17 DIV were subjected to calcium imaging. Several of the KO neurons were infected with the lentivirus expressing myc-CPEB3 on 12–13 DIV for the rescue experiment (KO + myc-CPEB3). The Fura2-AM-loaded neurons were treated as indicated. Representative calcium images before or after NMDA treatment are shown on the left. The change in $[Ca^{2+}]$ influx was monitored by the fluorescence ratio at 340/380 nm (F/F_0) and plotted against time. The data obtained from three independent cultures with ~250–300 neurons in each group were expressed as the mean ± SEM. The statistical difference in $[Ca^{2+}]$ influx induced by NMDA between groups was analyzed using Student's *t* test. Scale bars: 100 mm.

seen in the KOs. It is possible that dysregulation of other CPEB3-targeted RNAs may also contribute to the behavioral deficits. Identification of other mRNAs bound by CPEB3 using the UV-cross-linking procedure coupled with high throughout sequencing (HITS-CLIP) (Ule et al., 2003; Licatalosi et al., 2008) is currently in progress.

Multilayered controls of PRP syntheses

Accumulating evidence suggests syntheses of many PRPs are subject to multilayered post-transcriptional control with concerted actions of multiple RNA-binding proteins. For example, PSD95 is transcribed early in the mouse embryonic brain, although most of its product transcripts are degraded through polypyrimidine tract binding protein (PTBP)1 and PTBP2-regulated alternative splicing to trigger NMD (Zheng et al., 2012). The gradual loss of PTBP1 and PTBP2 during neuronal development allowed for the late expression of PSD95 during neuronal maturation. In contrast, CPEB3 level was low at the early stages during axonal and dendritic growth, and plateaued at the time of spine maturation when PSD95 expression began to upregulate in the KO neurons. The stability of PSD95 RNA is enhanced by fragile X mental retardation protein (FMRP) and metabotropic glutamate receptor (mGluR) activation (Zalfa et al., 2007). Moreover, FMRP can repress PSD95 translation through miR-125a; while mGluR activation alleviates this repression (Muddashetty et al., 2011). In addition to PSD95 RNA, the syntheses of GluA1, NR1, NR2A, and NR2B are also regulated by other RNA-binding proteins in addition to CPEB3 as well as many microRNAs (miRs). For instance, the genetic deletion of eIF-4E binding protein 2 (4E-BP2) in mice upregulates translation of GluA1 and GluA2 RNAs as judged by the distribution of GluA1 and GluA2 RNAs migrating toward the polysomal fractions of heavier density (Ran et al., 2013). NR2A was recently reported to be regulated through CPEB1-mediated polyadenylation-induced translation under the protocol used to stimulate chemical LTP in neurons (Udagawa et al., 2012; Swanger et al., 2013). Furthermore, altered expression levels of several miRs, such as miR-124 (Dutta et al., 2013), miR-132, miR-181a (Saba et al., 2012), and miR-223 (Harraz et al., 2012) could directly or indirectly influence the protein levels of some subunits of AMPARs and/or NMDARs. In addition to the previously identified GluA1 and GluA2 RNAs, this study has identified that CPEB3 also plays a role in confining the translation of PSD95 and NMDAR subunit RNAs, suggesting that multilayered control of these PRP syntheses is critical for synaptic plasticity, learning, and memory.

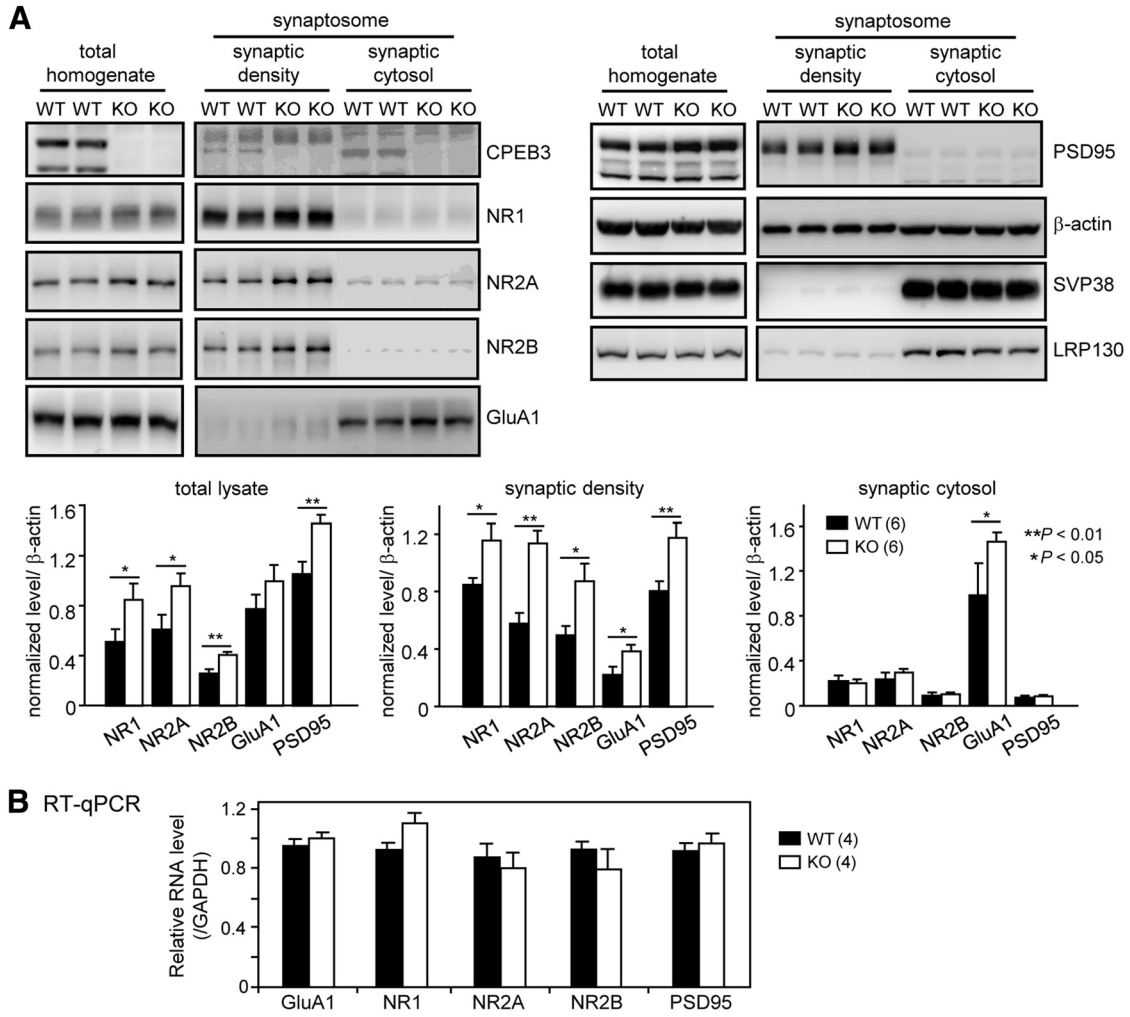

Figure 8. Deletion of CPEB3 resulted in increased total and synaptic protein levels of PSD95 and NMDAR. ***A***, The total homogenates and synaptosomal fractions (synaptic density and synaptic cytosol) were isolated from 3-month-old WT and KO mouse brains ($n = 6$ in each group) and used for Western blotting analysis. The protein levels of NR1, NR2A, NR2B, GluA1, and PSD95 were normalized against β-actin. Synaptophysin (SVP38) and leucine-rich protein (LRP)130 served as nontarget controls. The quantified data were expressed as the mean ± SEM in the bar graphs. Significant differences between the WT and KO groups are denoted as $^{*}p < 0.05$ or $^{**}p < 0.01$, Student's *t* test. ***B***, The relative expression levels of various RNAs in WT and KO brains were similar. The cortices and hippocampi isolated from the 3-month-old WT and KO mice (4 animals in each genotype) were extracted for RNAs. The total RNAs were then reverse-transcribed and processed for RT-qPCR.

Are CPEBs functionally redundant in learning and memory?

Vertebrates contain four *cpeb* genes and all of them encode proteins widely expressed in the brain including the hippocampal area (Theis et al., 2003). The RBD of CPEB1 has a higher sequence identity to *Drosophila* CPEB1 (i.e., Orb, 60%) and *Aplysia* CPEB (ApCPEB, 65%) compared with CPEBs 2–4 (45%). CPEBs 2–4 are 96% identical in this region and have 87% identity with their fly homolog, Orb2 (Fig. 10). Swapping the RBDs between CPEB1 and CPEB3 in *Xenopus* oocytes or Orb and Orb2 in the fly along with the *in vitro* RNA-binding assay all indicate that CPEB1 (Orb) and CPEB-like proteins (CPEBs 2–4 and Orb2) possess distinct sequence preference for binding and likely regulate different spectrums of RNAs *in vivo* (Huang et al., 2006; Krüttner et al., 2012). In contrast to the C-terminal RBD, only CPEBs 2–4 have ~25–35% identity among themselves, but show no significant homology with CPEB1, ApCPEB, and Orb2 in the N-terminal region (Fig. 10). The CPEB2 isoform used for comparison here is CPEB2a, which is the most abundantly expressed in neurons (Chen and Huang, 2012). In the present study, we showed the behavioral defects in CPEB3-deficient mice are clearly different from CPEB1-null mice. Particularly, CPEB1-dependent protein synthesis is an important cellular mechanism underlying extinction of hippocampus-dependent memories in both contextual fear memory and water maze spatial memory (Berger-Sweeney et al., 2006). In contrast, CPEB3 is more involved in confining the strength of consolidated spatial memory in the water maze task. The increased expression of multiple glutamatergic synapse molecules also affects short-term contextual fear memory, which is a protein synthesis-independent process. With the exception of NR2A RNA, all other CPEB3-bound RNAs identified from this study have not been reported to be regulated by CPEB1. Thus, it appears that different CPEB members may participate in establishing memory of specific kind. The mechanisms underlying memory extinction, while also requiring new protein production, can be somewhat distinct from those underlying consolidation, storage, and retrieval of memories. Although Orb2 is necessarily required for consolidating long-term courtship memory in the fly (Keleman et al., 2007), one of its mammalian homologs, CPEB3, seems to be dispensable for forming long-term spatial memory. The contribution of CPEB2

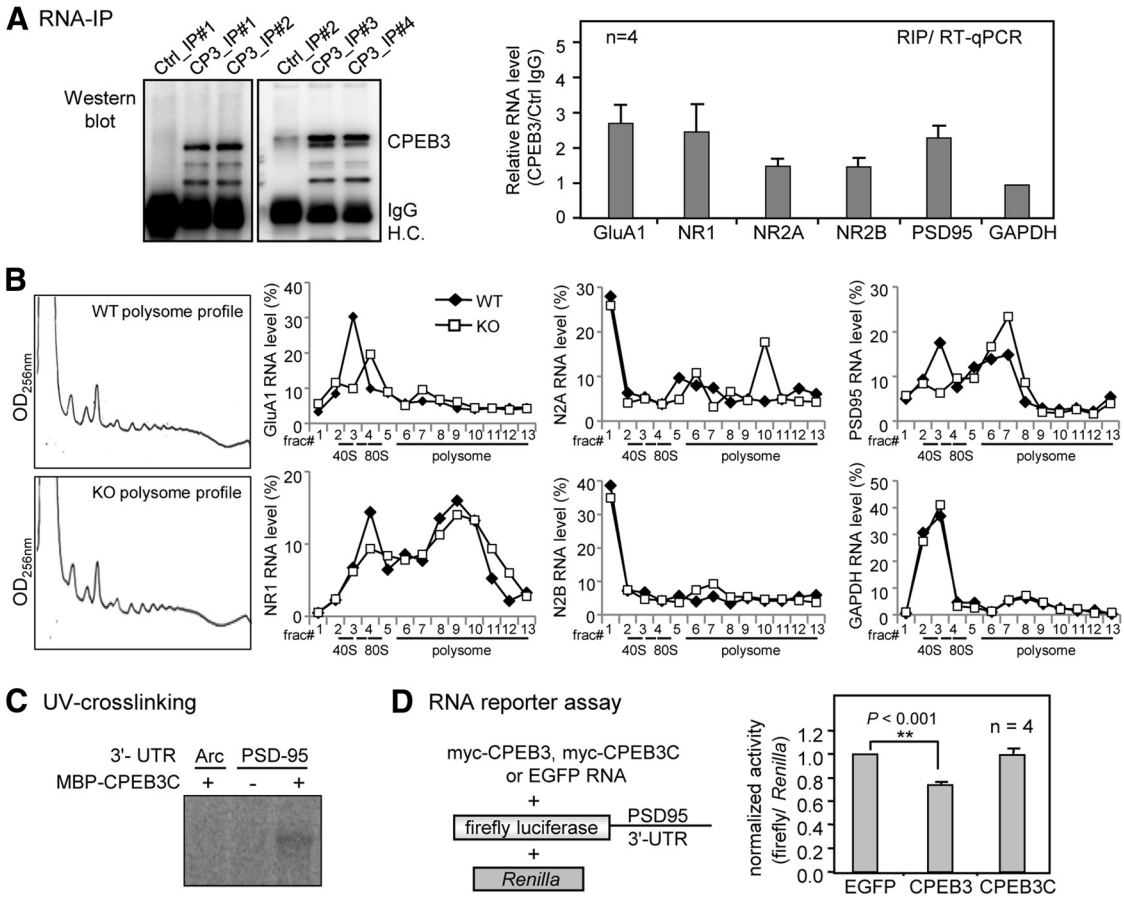

Figure 9. CPEB3 binds to the PSD95 RNA and represses its translation. ***A***, RIP. The mouse brain lysate was immunoprecipitated with control or CPEB3 IgG. The precipitated RNAs were reverse transcribed followed by RT-qPCR to determine the relative RNA levels between control and CPEB3 immunoprecipitates. ***B***, The polysomal profiles of WT and CPEB3 KO neurons are shown on the left. The polysomal distribution of GluA1, NR1, NR2A, NR2B, PSD95, and the control GAPDH RNAs in WT and KO neurons was determined by RT-qPCR using RNAs isolated from each fraction and expressed as the percentage of total RNAs summed from all fractions. ***C***, CPEB3 bound to PSD95 3′-UTR. The recombinant maltose binding protein (MBP) fused to the C terminus of CPEB3 RBD (MBP-CPEB3C) was UV-cross-linked with ^{32}P-labeled 3′-UTRs of Arc and PSD95 RNAs, RNase treated, and then analyzed by SDS-PAGE. ***D***, RNA reporter assay. The cultured neurons were transfected with RNAs encoding myc-CPEB3, myc-CPEB3C, or EGFP, in combination with the firefly luciferase appended to the PSD95 3′-UTR and *Renilla* luciferase. The normalized luciferase activity (firefly/*Renilla*) was calculated. Four independent results were analyzed and expressed as the mean ± SEM. Asterisks mark the significant difference (Student's *t* test).

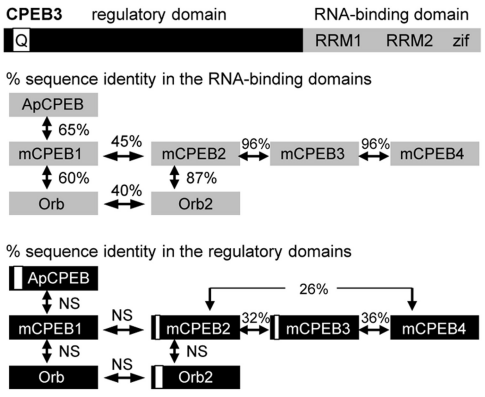

Figure 10. Sequence comparison of CPEB family proteins. All CPEB proteins have an N-terminal region (black box) and a C-terminal region (gray box) containing two RNA recognition motifs (RRM) and two zinc fingers (Zif). Among the RBDs, there is considerable identity ranging from 40 to 96%. Mouse CPEBs 2–4 are nearly identical in the RBDs. Mouse CPEB1 (mCPEB1) is closer to *Aplysia* CPEB (ApCPEB) and *Drosophila* CPEB (Orb) than it is to mCPEB2; in addition, *Drosophila* Orb2 is more similar to mCPEBs 2–4 than it is to Orb. Except for CPEBs 2–4, there is little identity (NS, not significant) among the N-terminal regions of the CPEB proteins. Moreover, the Q-rich sequence of variable length (white box) is present in some CPEB proteins.

and CPEB4 in learning and memory will require further investigation by first establishing the KO mice.

Are mammalian CPEBs prions?

A critical question regarding long-term synaptic plasticity is how to sensitize and potentiate naive synapses once stimulated and how a transient activation by the presynaptic release of neurotransmitters achieves prolonged synaptic modifications. It has been known for decades that activity-induced synthesis of PRPs is crucial for the establishment and consolidation of LTM, but how these newly synthesized proteins with a half-life of hours or days can maintain synaptic strength and persist life-long memory are unclear. Studies in *Aplysia* and *Drosophila* have postulated a prion-like translational regulator, CPEB, which may offer a solution to this conundrum (Si et al., 2010; Krüttner et al., 2012; Majumdar et al., 2012). "Prion-like mechanism in LTM" proposes that an initial conformational change of a translational repressor in response to synaptic stimulation can template the conversion of other soluble proteins into a prion-dominant conformation. Once converted to a self-perpetuating prion form, this repressor becomes a translational activator that continuously supplies proteins required for the generation of stable synapses and memory (Si et al., 2010). Although a few studies have shown

that prion-like oligomerization of Orb2 can be activity induced and was essential for LTM of the fly courtship behavior (Krüttner et al., 2012; Majumdar et al., 2012), it remains largely unknown how the physical conversion of Orb2 from a soluble to a prion structure changes its function from a repressor (Mastushita-Sakai et al., 2010) to an activator. Mammals express four CPEBs in neurons, but only CPEB2 and CPEB3 contain short Q-stretch motifs in the N terminus. Although the prion domain in Orb2 can be substituted with the Q-containing motif from mouse CPEB3 (Krüttner et al., 2012), in this study, CPEB3 KO mice displayed a potentiated short-term fear response in contextual fear conditioning and enhanced long-term spatial memory in the MWZ, indicating that CPEB3 unlikely employs a prion-like mechanism to persist in all types of long-term memories. Biochemical studies also supported a role of CPEB3 as a translational repressor (Huang et al., 2006) to constrain the expressions of AMPAR, PSD95, and NMDAR. Although CPEB3 KO mice have better spatial memory in the MWZ, such potentiated memory appears to jeopardize their ability to rapidly acquire new spatial information during reversal learning, suggesting that a slight alteration in the synaptic proteome composition could shift the balance of learning and memory toward a better response for one task and a worse response for the other. Whether CPEB3 may employ a prion-like mechanism to influence specific kinds of memories or other mammalian homologs of Orb2 (i.e., CPEB2 and CPEB4) can employ a prion-like mechanism to positively regulate learning and memory, will require further investigation.

References

Alarcon JM, Hodgman R, Theis M, Huang YS, Kandel ER, Richter JD (2004) Selective modulation of some forms of schaffer collateral-CA1 synaptic plasticity in mice with a disruption of the CPEB-1 gene. Learn Mem 11:318–327. CrossRef Medline

Béïque JC, Lin DT, Kang MG, Aizawa H, Takamiya K, Huganir RL (2006) Synapse-specific regulation of AMPA receptor function by PSD-95. Proc Natl Acad Sci U S A 103:19535–19540. CrossRef Medline

Berger-Sweeney J, Zearfoss NR, Richter JD (2006) Reduced extinction of hippocampal-dependent memories in CPEB knock-out mice. Learn Mem 13:4–7. CrossRef Medline

Brigman JL, Wright T, Talani G, Prasad-Mulcare S, Jinde S, Seabold GK, Mathur P, Davis MI, Bock R, Gustin RM, Colbran RJ, Alvarez VA, Nakazawa K, Delpire E, Lovinger DM, Holmes A (2010) Loss of GluN2B-containing NMDA receptors in CA1 hippocampus and cortex impairs long-term depression, reduces dendritic spine density, and disrupts learning. J Neurosci 30:4590–4600. CrossRef Medline

Chao HW, Hong CJ, Huang TN, Lin YL, Hsueh YP (2008) SUMOylation of the MAGUK protein CASK regulates dendritic spinogenesis. J Cell Biol 182:141–155. CrossRef Medline

Chao HW, Lai YT, Lu YL, Lin CL, Mai W, Huang YS (2012) NMDAR signaling facilitates the IPO5-mediated nuclear import of CPEB3. Nucleic Acids Res 40:8484–8498. CrossRef Medline

Chen PJ, Huang YS (2012) CPEB2-eEF2 interaction impedes HIF-1alpha RNA translation. EMBO J 31:959–971. Medline

Chourbaji S, Vogt MA, Fumagalli F, Sohr R, Frasca A, Brandwein C, Hörtnagl H, Riva MA, Sprengel R, Gass P (2008) AMPA receptor subunit 1 (GluR-A) knockout mice model the glutamate hypothesis of depression. FASEB J 22:3129–3134. CrossRef Medline

Costa-Mattioli M, Sossin WS, Klann E, Sonenberg N (2009) Translational control of long-lasting synaptic plasticity and memory. Neuron 61:10–26. CrossRef Medline

Cui Z, Feng R, Jacobs S, Duan Y, Wang H, Cao X, Tsien JZ (2013) Increased NR2A:NR2B ratio compresses long-term depression range and constrains long-term memory. Sci Rep 3:1036. Medline

Cull-Candy S, Brickley S, Farrant M (2001) NMDA receptor subunits: diversity, development and disease. Curr Opin Neurobiol 11:327–335. CrossRef Medline

Darnell JC, Richter JD (2012) Cytoplasmic RNA-binding proteins and the control of complex brain function. Cold Spring Harb Perspect Biol 4:a012344. CrossRef Medline

Dong YN, Waxman EA, Lynch DR (2004) Interactions of postsynaptic density-95 and the NMDA receptor 2 subunit control calpain-mediated cleavage of the NMDA receptor. J Neurosci 24:11035–11045. CrossRef Medline

Dutta R, Chomyk AM, Chang A, Ribaudo MV, Deckard SA, Doud MK, Edberg DD, Bai B, Li M, Baranzini SE, Fox RJ, Staugaitis SM, Macklin WB, Trapp BD (2013) Hippocampal demyelination and memory dysfunction are associated with increased levels of the neuronal microRNA miR-124 and reduced AMPA receptors. Ann Neurol 73:637–645. CrossRef Medline

Ehrlich I, Klein M, Rumpel S, Malinow R (2007) PSD-95 is required for activity-driven synapse stabilization. Proc Natl Acad Sci U S A 104:4176–4181. CrossRef Medline

Gal-Ben-Ari S, Kenney JW, Ounalla-Saad H, Taha E, David O, Levitan D, Gildish I, Panja D, Pai B, Wibrand K, Simpson TI, Proud CG, Bramham CR, Armstrong JD, Rosenblum K (2012) Consolidation and translation regulation. Learn Mem 19:410–422. CrossRef Medline

Harraz MM, Eacker SM, Wang X, Dawson TM, Dawson VL (2012) MicroRNA-223 is neuroprotective by targeting glutamate receptors. Proc Natl Acad Sci U S A 109:18962–18967. CrossRef Medline

Huang YS, Kan MC, Lin CL, Richter JD (2006) CPEB3 and CPEB4 in neurons: analysis of RNA-binding specificity and translational control of AMPA receptor GluR2 mRNA. EMBO J 25:4865–4876. CrossRef Medline

Irvine EE, Drinkwater L, Radwanska K, Al-Qassab H, Smith MA, O'Brien M, Kielar C, Choudhury AI, Krauss S, Cooper JD, Withers DJ, Giese KP (2011) Insulin receptor substrate 2 is a negative regulator of memory formation. Learn Mem 18:375–383. CrossRef Medline

Jia Z, Agopyan N, Miu P, Xiong Z, Henderson J, Gerlai R, Taverna FA, Velumian A, MacDonald J, Carlen P, Abramow-Newerly W, Roder J (1996) Enhanced LTP in mice deficient in the AMPA receptor GluR2. Neuron 17:945–956. CrossRef Medline

Keleman K, Krüttner S, Alenius M, Dickson BJ (2007) Function of the Drosophila CPEB protein Orb2 in long-term courtship memory. Nat Neurosci 10:1587–1593. CrossRef Medline

Kemp N, McQueen J, Faulkes S, Bashir ZI (2000) Different forms of LTD in the CA1 region of the hippocampus: role of age and stimulus protocol. Eur J Neurosci 12:360–366. CrossRef Medline

Krüttner S, Stepien B, Noordermeer JN, Mommaas MA, Mechtler K, Dickson BJ, Keleman K (2012) Drosophila CPEB Orb2A mediates memory independent of Its RNA-binding domain. Neuron 76:383–395. CrossRef Medline

Licatalosi DD, Mele A, Fak JJ, Ule J, Kayikci M, Chi SW, Clark TA, Schweitzer AC, Blume JE, Wang X, Darnell JC, Darnell RB (2008) HITS-CLIP yields genome-wide insights into brain alternative RNA processing. Nature 456:464–469. CrossRef Medline

Majumdar A, Cesario WC, White-Grindley E, Jiang H, Ren F, Khan MR, Li L, Choi EM, Kannan K, Guo F, Unruh J, Slaughter B, Si K (2012) Critical role of amyloid-like oligomers of Drosophila Orb2 in the persistence of memory. Cell 148:515–529. CrossRef Medline

Mastushita-Sakai T, White-Grindley E, Samuelson J, Seidel C, Si K (2010) Drosophila Orb2 targets genes involved in neuronal growth, synapse formation, and protein turnover. Proc Natl Acad Sci U S A 107:11987–11992. CrossRef Medline

Masuya H, Inoue M, Wada Y, Shimizu A, Nagano J, Kawai A, Inoue A, Kagami T, Hirayama T, Yamaga A, Kaneda H, Kobayashi K, Minowa O, Miura I, Gondo Y, Noda T, Wakana S, Shiroishi T (2005) Implementation of the modified-SHIRPA protocol for screening of dominant phenotypes in a large-scale ENU mutagenesis program. Mamm Genome 16:829–837. CrossRef Medline

Migaud M, Charlesworth P, Dempster M, Webster LC, Watabe AM, Makhinson M, He Y, Ramsay MF, Morris RG, Morrison JH, O'Dell TJ, Grant SG (1998) Enhanced long-term potentiation and impaired learning in mice with mutant postsynaptic density-95 protein. Nature 396:433–439. CrossRef Medline

Morgan M, Iaconcig A, Muro AF (2010) CPEB2, CPEB3 and CPEB4 are coordinately regulated by miRNAs recognizing conserved binding sites in paralog positions of their 3′-UTRs. Nucleic Acids Res 38:7698–7710. CrossRef Medline

Morris R (1984) Developments of a water-maze procedure for studying spatial learning in the rat. J Neurosci Methods 11:47–60. CrossRef Medline

Muddashetty RS, Nalavadi VC, Gross C, Yao X, Xing L, Laur O, Warren ST, Bassell GJ (2011) Reversible inhibition of PSD-95 mRNA translation by miR-125a, FMRP phosphorylation, and mGluR signaling. Mol Cell 42: 673–688. CrossRef Medline

Oliet SH, Malenka RC, Nicoll RA (1997) Two distinct forms of long-term depression coexist in CA1 hippocampal pyramidal cells. Neuron 18:969–982. CrossRef Medline

Patterson SL, Pittenger C, Morozov A, Martin KC, Scanlin H, Drake C, Kandel ER (2001) Some forms of cAMP-mediated long-lasting potentiation are associated with release of BDNF and nuclear translocation of phospho-MAP kinase. Neuron 32:123–140. CrossRef Medline

Pavlopoulos E, Trifilieff P, Chevaleyre V, Fioriti L, Zairis S, Pagano A, Malleret G, Kandel ER (2011) Neuralized1 activates CPEB3: a function for nonproteolytic ubiquitin in synaptic plasticity and memory storage. Cell 147:1369–1383. CrossRef Medline

Peng SC, Lai YT, Huang HY, Huang HD, Huang YS (2010) A novel role of CPEB3 in regulating EGFR gene transcription via association with Stat5b in neurons. Nucleic Acids Res 38:7446–7457. CrossRef Medline

Ran I, Gkogkas CG, Vasuta C, Tartas M, Khoutorsky A, Laplante I, Parsyan A, Nevarko T, Sonenberg N, Lacaille JC (2013) Selective regulation of GluA subunit synthesis and AMPA receptor-mediated synaptic function and plasticity by the translation repressor 4E-BP2 in hippocampal pyramidal cells. J Neurosci 33:1872–1886. CrossRef Medline

Richter JD, Klann E (2009) Making synaptic plasticity and memory last: mechanisms of translational regulation. Genes Dev 23:1–11. CrossRef Medline

Saba R, Störchel PH, Aksoy-Aksel A, Kepura F, Lippi G, Plant TD, Schratt GM (2012) Dopamine-regulated microRNA MiR-181a controls GluA2 surface expression in hippocampal neurons. Mol Cell Biol 32:619–632. CrossRef Medline

Schoenberg DR, Maquat LE (2012) Regulation of cytoplasmic mRNA decay. Nat Rev Genet 13:246–259. CrossRef Medline

Shimizu E, Tang YP, Rampon C, Tsien JZ (2000) NMDA receptor-dependent synaptic reinforcement as a crucial process for memory consolidation. Science 290:1170–1174. CrossRef Medline

Si K, Choi YB, White-Grindley E, Majumdar A, Kandel ER (2010) Aplysia CPEB can form prion-like multimers in sensory neurons that contribute to long-term facilitation. Cell 140:421–435. CrossRef Medline

Swanger SA, He YA, Richter JD, Bassell GJ (2013) Dendritic GluN2A synthesis mediates activity-induced NMDA receptor insertion. J Neurosci 33:8898–8908. CrossRef Medline

Tang YP, Shimizu E, Dube GR, Rampon C, Kerchner GA, Zhuo M, Liu G, Tsien JZ (1999) Genetic enhancement of learning and memory in mice. Nature 401:63–69. CrossRef Medline

Theis M, Si K, Kandel ER (2003) Two previously undescribed members of the mouse CPEB family of genes and their inducible expression in the principal cell layers of the hippocampus. Proc Natl Acad Sci U S A 100: 9602–9607. CrossRef Medline

Tsien JZ, Huerta PT, Tonegawa S (1996) The essential role of hippocampal CA1 NMDA receptor-dependent synaptic plasticity in spatial memory. Cell 87:1327–1338. CrossRef Medline

Udagawa T, Swanger SA, Takeuchi K, Kim JH, Nalavadi V, Shin J, Lorenz LJ, Zukin RS, Bassell GJ, Richter JD (2012) Bidirectional control of mRNA translation and synaptic plasticity by the cytoplasmic polyadenylation complex. Mol Cell 47:253–266. CrossRef Medline

Ule J, Jensen KB, Ruggiu M, Mele A, Ule A, Darnell RB (2003) CLIP identifies Nova-regulated RNA networks in the brain. Science 302:1212–1215. CrossRef Medline

von Engelhardt J, Doganci B, Jensen V, Hvalby Ø, Göngrich C, Taylor A, Barkus C, Sanderson DJ, Rawlins JN, Seeburg PH, Bannerman DM, Monyer H (2008) Contribution of hippocampal and extra-hippocampal NR2B-containing NMDA receptors to performance on spatial learning tasks. Neuron 60:846–860. CrossRef Medline

Wang CF, Huang YS (2012) Calpain 2 activated through N-methyl-D-aspartic acid receptor signaling cleaves CPEB3 and abrogates CPEB3-repressed translation in neurons. Mol Cell Biol 32:3321–3332. CrossRef Medline

Wiedholz LM, Owens WA, Horton RE, Feyder M, Karlsson RM, Hefner K, Sprengel R, Celikel T, Daws LC, Holmes A (2008) Mice lacking the AMPA GluR1 receptor exhibit striatal hyperdopaminergia and 'schizophrenia-related' behaviors. Mol Psychiatry 13:631–640. CrossRef Medline

Zalfa F, Eleuteri B, Dickson KS, Mercaldo V, De Rubeis S, di Penta A, Tabolacci E, Chiurazzi P, Neri G, Grant SG, Bagni C (2007) A new function for the fragile X mental retardation protein in regulation of PSD-95 mRNA stability. Nat Neurosci 10:578–587. CrossRef Medline

Zheng S, Gray EE, Chawla G, Porse BT, O'Dell TJ, Black DL (2012) PSD-95 is post-transcriptionally repressed during early neural development by PTBP1 and PTBP2. Nat Neurosci 15:381–388:S1. Medline